SPECIAL
CCSM Earth System Model CESM1
COLLECTION

Climate Change Projections in CESM1(CAM5) Compared to CCSM4

Gerald A. Meehl and Warren M. Washington

National Center for Atmospheric Research,* Boulder, Colorado

Julie M. Arblaster

National Center for Atmospheric Research,* Boulder, Colorado, and CAWCR, Bureau of Meteorology, Melbourne, Australia

Aixue Hu, Haiyan Teng, Jennifer E. Kay, Andrew Gettelman, David M. Lawrence, Benjamin M. Sanderson, and Warren G. Strand

National Center for Atmospheric Research,* Boulder, Colorado

ABSTRACT

Future climate change projections for phase 5 of the Coupled Model Intercomparison Project (CMIP5) are presented for the Community Earth System Model version 1 that includes the Community Atmospheric Model version 5 [CESM1(CAM5)]. These results are compared to the Community Climate System Model, version 4 (CCSM4) and include simulations using the representative concentration pathway (RCP) mitigation scenarios, and extensions for those scenarios beyond 2100 to 2300. Equilibrium climate sensitivity of CESM1 (CAM5) is 4.10°C, which is higher than the CCSM4 value of 3.20°C. The transient climate response is 2.33°C, compared to the CCSM4 value of 1.73°C. Thus, even though CESM1(CAM5) includes both the direct and indirect effects of aerosols (CCSM4 had only the direct effect), the overall climate system response including forcing and feedbacks is greater in CESM1(CAM5) compared to CCSM4. The Atlantic Ocean meridional overturning circulation (AMOC) in CESM1(CAM5) weakens considerably in the twenty-first century in all the RCP scenarios, and recovers more slowly in the lower forcing scenarios. The total aerosol optical depth (AOD) changes from ~0.12 in 2006 to ~0.10 in 2100, compared to a preindustrial 1850 value of 0.08, so there is less negative forcing (a net positive forcing) from that source during the twenty-first century. Consequently, the change from 2006 to 2100 in aerosol direct forcing in CESM1(CAM5) contributes to greater twenty-first century warming relative to CCSM4. There is greater Arctic warming and sea ice loss in CESM1(CAM5), with an ice-free summer Arctic occurring by about 2060 in RCP8.5 (2040s in September) as opposed to about 2100 in CCSM4 (2060s in September).

1. Introduction

This paper describes results for the set of experiments from phase 5 of the Coupled Model Intercomparison Project (CMIP5; Taylor et al. 2012) for the Community Earth System Model version 1 (CESM1) that includes the Community Atmospheric Model version 5 (CAM5), referred to herein as CESM1(CAM5) (Neale et al. 2010). Results are presented for simulations of twenty-first-century climate with the four RCP scenarios, and extensions of the climate change projections from 2100 to 2300. Comparisons will be made to the previous model version, the Community Climate System Model, version 4 (CCSM4; Meehl et al. 2012a). As in that previous paper, the purpose of the present paper is to provide a general description of the simulation characteristics of the climate change projections made with CESM1(CAM5). This paper is part of a CESM1 special collection and is intended to provide background and documentation of simulation features that can be used as a reference for

subsequent papers that will examine in detail the processes and mechanisms involved with producing the projection results shown here.

Section 2 includes a short description of the model and experiments. Section 3 presents results from the climate change projections from the twenty-first century using the RCP scenarios, as well as the extensions from 2100 to 2300. Projected changes in the AMOC are shown in section 4, while features of the climate change projections related to how aerosols are represented in CESM1 (CAM5) compared to CCSM4 are discussed in section 5. Projected changes of Arctic and Antarctic climate are described in section 6, while discussion and conclusions follow in sections 7 and 8, respectively.

2. Model and experiments

a. Model description

The CESM1(CAM5) has the same land, ocean (including an overflow parameterization), and sea ice components as in CCSM4 (Gent et al. 2011), with the biggest change occurring in the atmosphere. General features of the model formulation are given by Neale et al. (2010) and results for twentieth-century climate simulations are given by R. B. Neale et al. (2013, personal communication). The CAM5 is essentially a new atmospheric model with improved and more realistic formulations of radiation, boundary layer, and aerosols (R. B. Neale et al. 2013, personal communication). In particular, the aerosol scheme (Liu et al. 2012) is prognostic, and the cloud microphysics (Morrison and Gettelman 2008; Gettelman et al. 2010) includes both the direct and indirect effect for sulfate and black and organic carbon. More specifically, in CAM5 direct effects of aerosols are included in the radiation code. Indirect effects of aerosols are treated such that activated aerosol [as described by Gettelman et al. (2008)] affects the number concentration of cloud drops and ice crystals. Changing the condensate number impacts the resulting microphysical processes (such as sedimentation and auto conversion) as well as the radiative effects of these cloud drops. Since one of the criticisms of CCSM4 was that it did not include the aerosol indirect effect, its inclusion in CESM1(CAM5) represents a major improvement.

Another improvement that provides more realism is that there is time-evolving land use change in the twentieth- and twenty-first-century climate simulations (Lawrence et al. 2011). Those land use changes were shown by P. J. Lawrence et al. (2012) to not have large global effects, but to affect some regional climate regimes. Thus, the CESM1(CAM5) includes more realism and complexity and produces an improved

simulation of twentieth-century climate as a consequence (R. B. Neale et al. 2013, personal communication).

The resolution of CESM1(CAM5) is comparable to CCSM4, and includes a finite volume nominal 1° (0.9° × 1.25°) 30-level version of CAM5. The Parallel Ocean Program (POP) has 60 levels in the vertical, with the ocean grid points having a uniform 1.11° spacing in the zonal direction everywhere, while in the meridional direction, the resolution is 0.27° near the equator, extending to 0.54° poleward of 35°N and S and is constant at higher latitudes. As in CCSM4, no flux adjustments are used in CESM1(CAM5).

b. Future climate experiments

Experiments analyzed here for CESM1(CAM5) consist of three ensemble members (five ensemble members for CCSM4) for the future climate simulations that begin on 1 January 2006, for four mitigation scenarios termed representative concentration pathways (RCPs; Moss et al. 2010) and extend from the end of twentieth-century simulations. These scenarios represent classes of mitigation scenarios that produce emission pathways following various assumed policy decisions that would influence the time evolution of the future emissions of greenhouse gases (GHGs), aerosols, ozone, and land use/land cover change (Moss et al. 2010; van Vuuren et al. 2011).

As noted by Moss et al. (2010) and Meehl et al. (2012a), in the low scenario, RCP2.6, CO_2 emissions become negative by about 2070. Thus, more CO_2 would have to be removed from the atmosphere than is being put in, thereby achieving a decreasing trend in CO_2 concentrations by the end of the century. Although there are many ways to achieve this target, one way is to have global energy sources for human use consist of 20% fossil fuel without carbon capture and storage (CCS) by 2070 in addition to about 45% fossil fuel with CCS, 35% renewables (some of that includes biomass and CCS as well), and nuclear. In contrast, by 2070 in the high-emission scenario RCP8.5, for a comparable total net energy source, 80% of energy produced would use fossil fuels without CCS, with only 20% renewables and nuclear (van Vuuren et al. 2011).

The time evolution of GHGs, ozone recovery (i.e., as the ozone-destroying chemicals now banned by the Montreal Protocol are reduced, stratospheric ozone is projected to recover to mid-twentieth-century concentrations during the twenty-first century), and land use–cover are all specified in the respective RCPs (Lamarque et al. 2011) with aerosol concentrations computed by the atmospheric model from standardized gridded emissions (Lamarque et al. 2010). All RCPs have a similar evolution of ozone depleting substances, based on the

TABLE 1. Table of estimates of radiative fluxes from atmosphere-only model experiments. For each RCP, shown are global mean estimates of the changes (Δ) between simulations with 2100 and 2005 emissions for cloud radiative effect (CRE), top-of-atmosphere (TOA) radiation change minus the net flux in the shortwave for clear sky (FSC), the longwave cloud radiative effect (LWCRE), shortwave cloud radiative effect (SWCRE), the TOA and FSC changes (all in $W\,m^{-2}$), and the change in aerosol optical depth (AOD).

	ΔCRE	ΔTOA − ΔFSC	ΔLWCRE	ΔSWCRE	ΔTOA	ΔFSC	ΔAOD
RCP8.5	0.8	0.7	−0.4	1.3	0.9	0.3	−0.010
RCP6.0	1.0	1.0	−0.4	1.4	1.1	0.2	−0.010
RCP4.5	1.0	0.9	−0.2	1.3	1.3	0.4	−0.013
RCP2.6	1.2	1.1	−0.5	1.7	1.3	1.2	−0.012

Special Report on Emissions Scenarios (SRES) A1 halon scenario (Eyring et al. 2010, 2013). As was the case for CCSM4, CESM1(CAM5) includes the 11-yr solar cycle by repeating the last four solar cycles over the duration of all the RCP simulations, and volcanic aerosols are held constant at year 2005 values. The latter could of course produce somewhat of an overestimate of projected warming since there will be some volcanic eruptions during the twenty-first century. But because the location, timing, and magnitude of future volcanic eruptions are inherently unpredictable, their effects are not included. But in relative terms, this is likely not a big effect given the uncertainty of other future forcings.

In addition to these simulations, we also perform separate experiments to assess the aerosol forcing in CESM1(CAM5). These experiments are carried out using annually repeating monthly mean climatological SSTs and GHG emissions for the present day. Simulations are performed for aerosol precursor and oxidant emissions from 2005 and 2100 for each of the RCP cases. These runs permit an estimate of the direct and indirect effect of aerosols differences between the two emissions years. These special simulations are performed at a coarser $1.9° \times 2.5°$ horizontal resolution for 6 years for 2005 and 2100 conditions, with the last 5 years analyzed, to provide estimates of the aerosol forcings.

Global aerosol forcings for direct and indirect effects differ strongly between 2006 and 2100 as RCPs project a "cleanup" of aerosol emissions to the atmosphere, and results are presented in Table 1. Consistent with Lamarque et al. (2011), the total aerosol optical depth (AOD) changes from ~0.12 in 2006 to ~0.10 in 2100, compared to a preindustrial 1850 value of 0.08. Thus, as aerosol concentration drops over the twenty-first century, there is less negative forcing, which results in a net positive forcing. We estimate the direct effect as an increase of net top of atmosphere shortwave clear-sky flux (FSC) of $+0.2$ to $+0.4\,W\,m^{-2}$ in CESM1(CAM5) from 2006 to 2100. Lamarque et al. (2011) indicate that this corresponds to a similar value of about $+0.5\,W\,m^{-2}$ of additional forcing in CCSM4 that comes from a reduction of 60% in the direct anthropogenic cooling effects of

aerosols. Gettelman et al. (2012b) note a total indirect effect of $-1.3\,W\,m^{-2}$ in CESM1(CAM5) in 2000 compared to the preindustrial climate in 1850. Assuming this scales approximately with global AOD, this would represent an additional forcing from the indirect effect between 2006 and 2100 in CESM1(CAM5) of $\sim +1\,W\,m^{-2}$ that is not present in CCSM4 since CCSM4 does not include the indirect effect. Table 1 indicates a reduction of this indirect effect in CESM1(CAM5) from 2005 to 2100 produces a net positive forcing of between $+0.8$ and $+1.2\,W\,m^{-2}$, removing most of the anthropogenic cooling. Further discussion of the regional effects of aerosols is given in section 5 below.

As shown by Meehl et al. (2012a), the RCP scenarios are all extended from 2100 to 2300 from one of the ensemble members, with RCP4.5 and RCP6.0 stabilizing CO_2 concentrations by the early 2100s, while RCP8.5 does not level out until the mid-2200s. As noted above, after the mid-twenty-first century RCP2.6 has an ongoing slow decrease of CO_2 concentrations until there is virtually no time rate of change by the end of the twenty-third century.

c. Climate sensitivity

Typical metrics of model response include the equilibrium climate sensitivity (ECS) and the transient climate response (TCR). The ECS is traditionally computed in an experiment with an active atmospheric component coupled to a nondynamic slab ocean, where the CO_2 concentration doubles instantaneously and the model runs to equilibrium. The ECS is the difference in the globally averaged surface air temperature between the initial control run and the doubled-CO_2 equilibrium. This value is 4.10°C in CESM1(CAM5), compared to 3.20°C in CCSM4 (Meehl et al. 2012a; Bitz et al. 2012; Gettelman et al. 2012a; Kay et al. 2012). The radiative forcing for a doubling of CO_2 (with stratospheric adjustment but no tropospheric adjustment) is larger in CAM5 ($3.7\,W\,m^{-2}$) than in CAM4 ($3.5\,W\,m^{-2}$). Gettelman et al. (2012a) attribute about 40% of the difference in equilibrium forcing between the two models to CO_2 (Kay et al. 2012), and the remaining 60% to cloud feedbacks.

Thus the CESM1(CAM5) is somewhat more sensitive to increased CO_2 than the CCSM4. ECS values cited in the Intergovernmental Panel on Climate Change Fourth Assessment Report (IPCC AR4), obtained from multiple lines of modeling, observational, and paleoclimate evidence, range from 2.0° to 4.5°C, with a most likely mean value of about 3°C [see Meehl et al. (2007) for assumptions behind this assessment]. For the new CMIP5 multimodel ensemble, this range is 2.1° to 4.7°C (Andrews et al. 2012). Thus both CESM1(CAM5) and CCSM4 fall well within those ranges, with CESM1(CAM5) a bit higher than the most likely value. As noted above, the future transient simulations CESM1(CAM5) also experience an effective additional forcing of nearly +0.8 to +1.2 W m^{-2} due to the decline of aerosol concentrations after 2006. The greater sensitivity and greater forcing in CESM1(CAM5) compared to CCSM4 will characterize nearly all the results presented in this paper, with CESM1(CAM5) consistently producing greater magnitude climate changes as a consequence.

The TCR is computed from an experiment with a fully coupled model, branching from a control run, and increasing CO_2 at 1% yr^{-1} compounded. The TCR is the difference with the control of the 20-yr globally averaged surface air temperature centered on the time when CO_2 doubles, at roughly 70 years. The TCR is 2.33°C for CESM1(CAM5), compared to 1.73°C for CCSM4. For atmosphere–ocean coupled GCMs (AOGCMs) in the IPCC AR4, it was noted that the very likely range of TCR is about 1° to 3°C, with a mean TCR from the CMIP3 AOGCMs of 1.8°C (Meehl et al. 2007). Thus, the TCR values for CESM1(CAM5) and CCSM4 are close to those other estimates.

The increase of ECS in CESM1(CAM5) compared to CCSM4 is proportionately less (28%) than the increase in TCR (35%). This implies that transient ocean heat uptake must be reduced in CESM1(CAM5) compared to CCSM4 such that more heat is remaining in the atmosphere and not being taken up by the ocean as quickly. Indeed, this is the case, as will be discussed below (in relation to Fig. 3) to show that a reduced rate of ocean heat uptake contributes to somewhat greater transient warming in CESM1(CAM5) compared to CCSM4.

Another major contributor to the increased climate system response to external forcings in CESM1(CAM5) involves cloud feedbacks. Gettelman et al. (2012a) and Sanderson and Shell (2013) have both investigated global cloud and noncloud radiative feedbacks in CCSM4 and CESM1(CAM5) and have found that multiple processes are responsible for the increased climate sensitivity in the newer model. A large portion of this increased sensitivity can be attributed to reduced negative stratus and stratocumulus shortwave cloud feedbacks in the tropics and midlatitudes, and to increased stratus loss in the Southern Ocean in CAM5. In addition to stronger warming feedbacks in CESM1(CAM5), as noted above, a 10% increase in the top-of-atmosphere (TOA) carbon dioxide radiative forcing in CESM1(CAM5) over CCSM4 contributes to increased climate sensitivity in the newer model (Kay et al. 2012). At high northern latitudes a substantial decrease in optical depth of Arctic clouds in CESM1(CAM5) compared to CCSM4 (Kay et al. 2012) makes CESM1(CAM5) significantly more sensitive to surface albedo changes. Therefore, the net feedback due to snow and ice albedo feedback has increased by a factor of 1.5 compared to CCSM4. Finally, there are enhanced positive short wave cloud feedbacks in CESM1(CAM5), mostly having to do with complex interactions of the moist physics parameterizations (Gettelman et al. 2013) on the equatorward branches of the storm tracks and in the subtropics that contribute to greater climate sensitivity in CESM1(CAM5) compared to CCSM4.

d. Observations

Observed global surface temperatures considered shortly are from version 3 of the Hadley Centre–Climate Research Unit temperature dataset (HadCRUT3; Brohan et al. 2006). Monthly sea ice concentrations for the period 1979–2010 were obtained from the National Snow and Ice Data Center. These data are derived from the *Nimbus-7* Scanning Multichannel Microwave Radiometer and *Defense Meteorological Satellite Program* (*DMSP*)-*F8*, -*F11*, and -*F13* Special Sensor Microwave Imager radiances using the National Aeronautics and Space Administration (NASA) team algorithm (Cavalieri et al.1999).

3. Climate change projections for the twenty-first century

R. B. Neale et al. (2013, personal communication) show that CESM1(CAM5) follows the time evolution of twentieth-century globally averaged surface air temperatures better than CCSM4. As noted by Meehl et al. (2012a), CCSM4 was somewhat warmer than the observations over the last couple decades of the twentieth century. It was speculated that inclusion of only the direct effect (without the additional cooling effects of the indirect effect) produced this warmer twentieth-century climate. Having the indirect effect in CESM1(CAM5) would then contribute to a somewhat cooler twentieth-century climate and better agreement with the time evolution of globally averaged surface air temperatures (R. B. Neale et al. 2013, personal communication). However, with regard to future climate, the reduction in this negative forcing (effectively a positive forcing) and
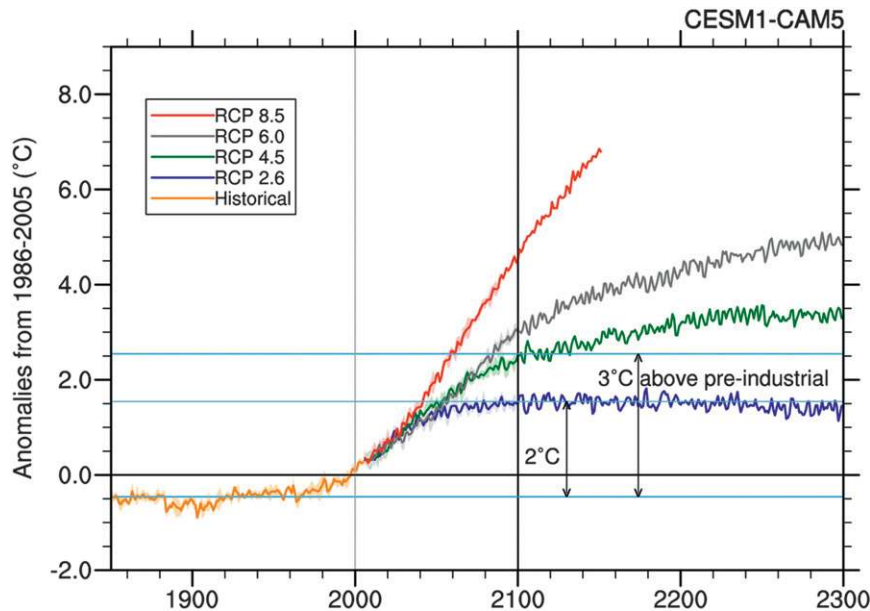
FIG. 1. Time series of annual globally averaged surface air temperature anomalies (relative to 1986–2005 base period; °C) from 1865 to 2300 for CESM1(CAM5). Solid lines with shading indicate ensemble average and ± one standard deviation of the ensemble members (three each for 1850–2100, and one each for the extensions beyond 2100). The year 2100 is denoted by vertical solid line, and there is lack of shading for standard deviations after 2100 since there is only 1 ensemble member, for RCP2.6, RCP4.5, RCP6.0, and RCP8.5.

the greater climate sensitivity of CESM1(CAM5) produces larger-amplitude warming than CCSM4. Figure 1 shows the time series of globally averaged surface air temperature for the CESM1(CAM5) ensemble mean of the twentieth-century all-forcings simulations and twenty-first-century RCP mitigation scenario simulations, and single member extensions to 2300 for each of the RCP scenarios. Figure 2 highlights the different responses of CESM1(CAM5) and CCSM4 for the four scenarios. The ensemble average warming for the last 20 years of the twenty-first century minus the period 1986–2005 for CESM1(CAM5) is +1.49°C for RCP2.6, +2.31°C for RCP4.5, +2.75°C for RCP6, and +4.13°C for RCP8.5, while those same differences for CCSM4 are +0.85°C for RCP2.6, +1.64°C for RCP4.5, +2.09°C for RCP6, and +3.53°C for RCP8.5.

Meehl et al. (2012a) noted that CCSM4 kept the warming below the 2°C above preindustrial target in RCP2.6. CESM1(CAM5), with its larger-amplitude response, barely keeps to the 2°C target as seen in Fig. 1. The difference is not just due to the climate sensitivity but is also a result of the additional twenty-first-century forcing of nearly ~1 W m^{-2} by reduction of the aerosol direct and indirect effects, while CCSM4 only accounts for the reduction of the direct effect (estimated at 0.2–0.4 W m^{-2} contributing to additional warming in the twenty-first century). In CCSM4, RCP4.5 stabilized near

a value of 3°C above preindustrial, but CESM1(CAM5) shows warming that is close to that value at 2100, and continues to increase to nearly 4°C above preindustrial by 2300.

Beyond the twenty-first century, RCP8.5 continues to warm with the ongoing increases of GHGs (Fig. 1). For RCP4.5, greenhouse gas concentrations effectively stabilize after 2100, but because of climate change commitment (e.g., Meehl et al. 2005) the climate system continues to warm such that the globally averaged surface air temperature difference for 2281–2300 (for that single member) minus 1986–2005 (for the historical ensemble member that corresponds to that single ensemble member extension) is +3.36°C. As noted above for RCP2.6, GHG concentrations slowly decrease after 2100, but in CESM1(CAM5) there is only small cooling compared to 2100 by 2300. The globally averaged surface air temperature difference for 2281–2300 (for that single member) minus 1986–2005 (for the historical ensemble member that corresponds to that single ensemble member extension) for RCP2.6 is +1.39°C, only somewhat lower than the ensemble average warming of +1.49°C for RCP2.6 given above for the last 20 years of the twenty-first century minus the period 1986–2005.

Thus, for CESM1(CAM5), the globally averaged surface air temperature changes post-twenty-first century
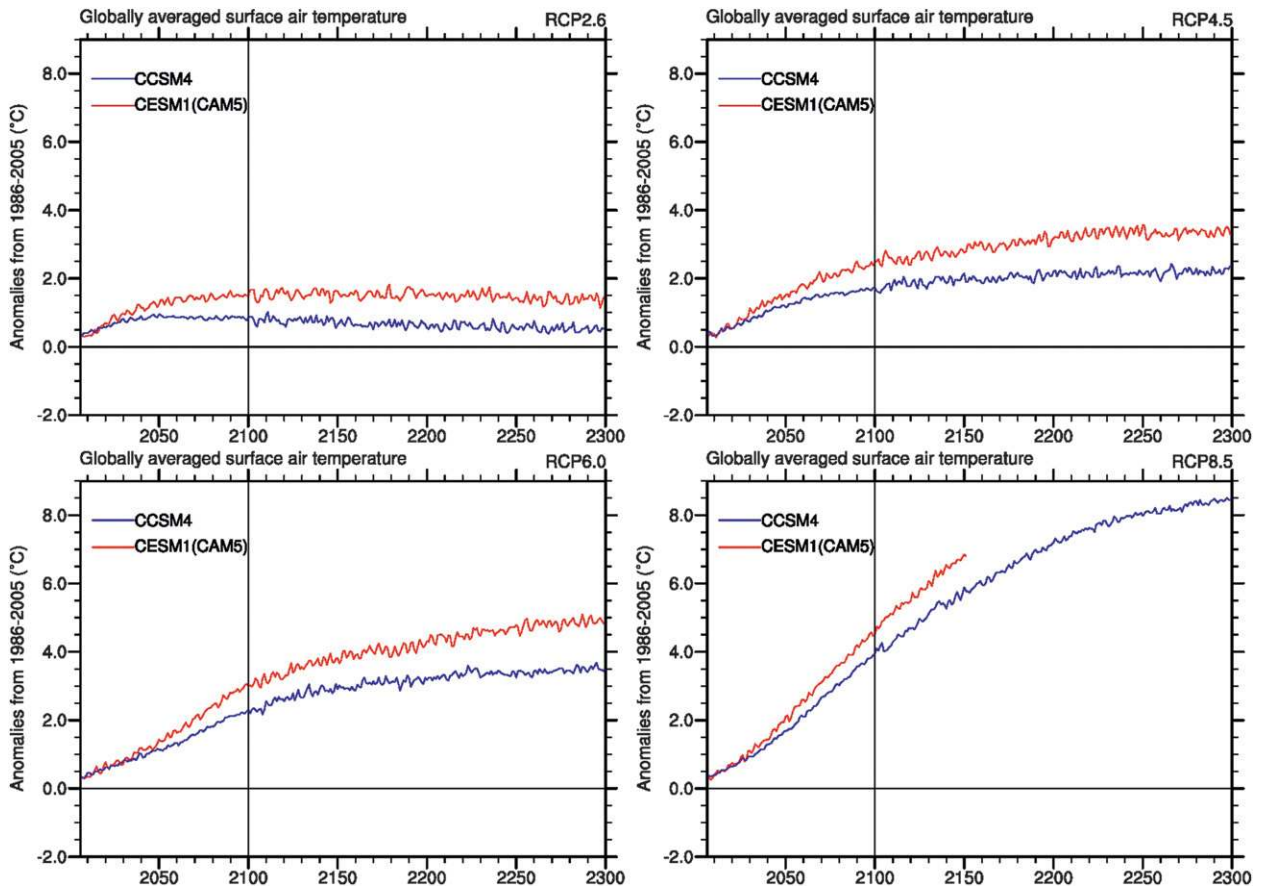
FIG. 2. Ensemble average time series of annual globally averaged surface air temperature anomalies (relative to 1986–2005 base period; °C) from 2006 to 2300 for CESM1(CAM5) (red line) and CCSM4 (blue line) for the four RCP scenarios indicated in the panel titles. The year 2100 is denoted by vertical solid line.

(2281–2300 minus 2081–2100 calculated for those single ensemble members) are −0.10°C for RCP2.6, +0.98°C for RCP4.5, and +2.03°C for RCP6.0.

As noted above, CESM1(CAM5) has a proportionately higher TCR increase than equilibrium climate sensitivity increase compared to CCSM4. This is because ocean heat uptake is slower in CESM1(CAM5), thus allowing a proportionately greater temperature increase in TCR compared to equilibrium climate sensitivity. This slower heat uptake also contributes, in a transient sense, to greater surface air temperature response in the RCP scenarios in Fig. 2. Some elements of ocean heat uptake, in the form of changes in ocean heat content, have been shown for CCSM4 in relation to sea level rise (Meehl et al. 2012b). Here we compare ocean heat content changes for the upper 300 m, 300 to 750 m, and below 750 m for both CCSM4 and CESM1(CAM5) in Fig. 3. Significant heat content increases are delayed about 100 years in all ocean layers in all scenarios in CESM1(CAM5) compared to CCSM4. This transient delay in ocean heat uptake is overcome with nearly equal

heat content increases by around 2100 in the upper 300 m in all scenarios, nearly catches up in the midocean layer, and is still lagging behind by 2100 in the deep ocean layers. Although the reasons for this difference in ocean heat uptake are the subject of a separate investigation, they are associated with reduced winds and a weaker AMOC in CESM1(CAM5) compared to CCSM4.

Geographical distributions of surface temperature difference patterns, CESM1(CAM5) minus CCSM4, are shown in Fig. 4 for the IPCC AR5 early-century time period (2016–35) and for late twenty-first century (2081–2100), for the four RCP scenarios. For the early-century period, the differences are negligible, with the biggest increase in relative warming in CESM1(CAM5) in the Arctic (see section 6 below). There are greater warming differences in CESM1(CAM5) for the late-century period in Fig. 4 in the Arctic as well as over the continental regions. Additionally, there is a temperature contrast near the deep water formation region at the confluence of the Labrador and Greenland Seas, with CESM1 (CAM5) being uncharacteristically colder.
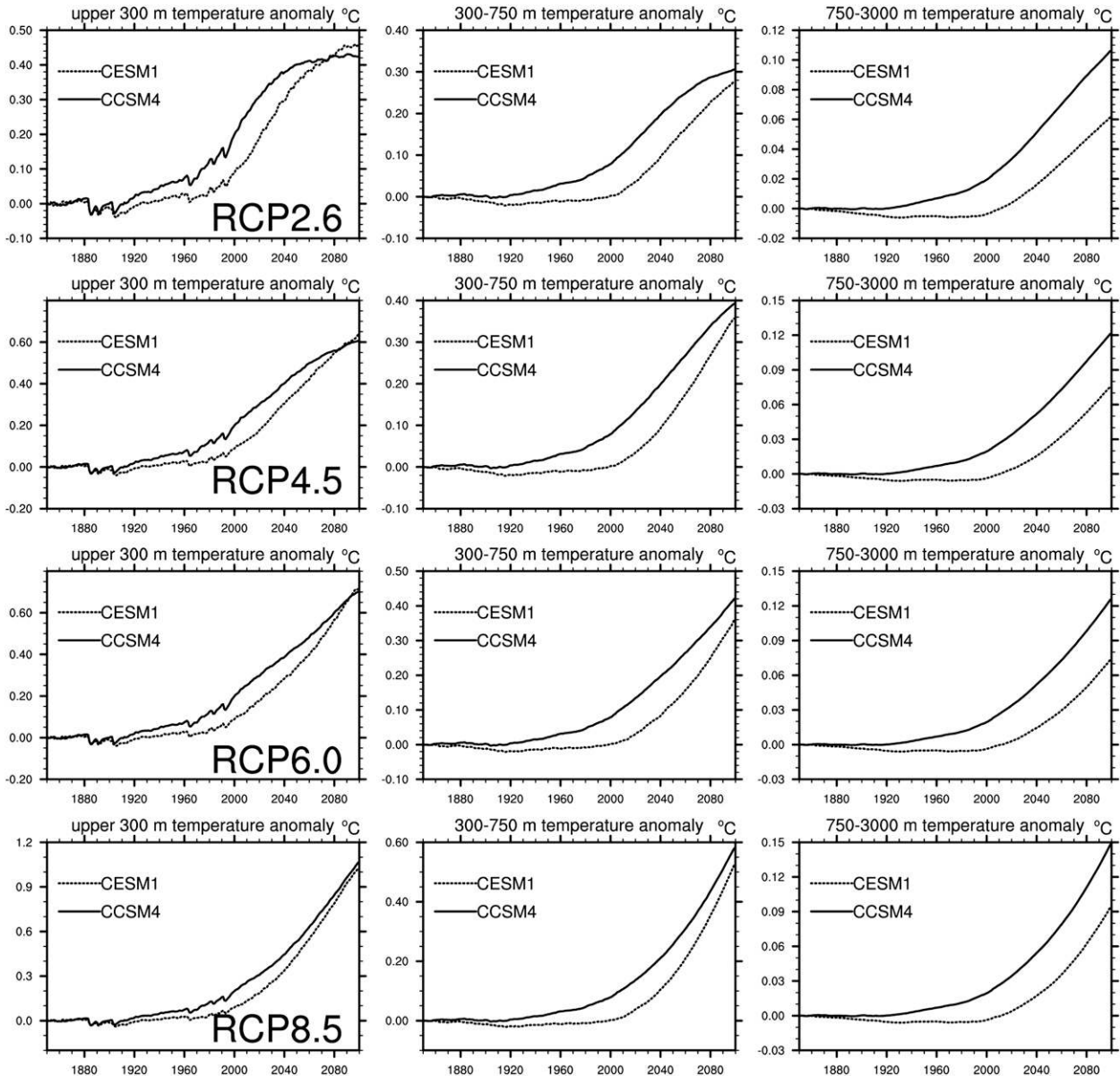
FIG. 3. Ocean heat content as represented by averaged ocean temperature anomalies (°C) for (left) the upper 300 m, (middle) 300–750 m, and (right) 750 m to bottom for (top) RCP2.6, (second row) RCP4.5, (third row) RCP6.0, and (bottom) RCP8.5 for CESM1 (CAM5) (dotted) and CCSM4 (solid).

Figure 5 shows geographical plots of December–February (DJF) and June–August (JJA) precipitation for CCSM4 and CESM1(CAM5) as differences for those two seasons for RCP8.5 for the 2081–2100 period at the end of the century minus the reference period 1986–2005. The other scenarios show similar patterns but with amplitudes of the differences roughly proportional to the forcing in the scenarios as shown in Fig. 4. There are greater precipitation increases in CESM1(CAM5) compared to CCSM4 that are particularly evident over the tropical Pacific in both seasons and the Mediterranean region in DJF. Given that SST anomalies are a combination of very small positive and negative changes (Fig. 4), the increases of precipitation in the tropical Pacific are likely a product of changes in CAM5, probably associated with boundary layer and cloud/radiation processes. There is relatively more precipitation in CESM1(CAM5) over the Arctic and many midlatitude areas in DJF as well as in the tropical Pacific and Indian Oceans, with some relative decreases in some subtropical areas. Zonal
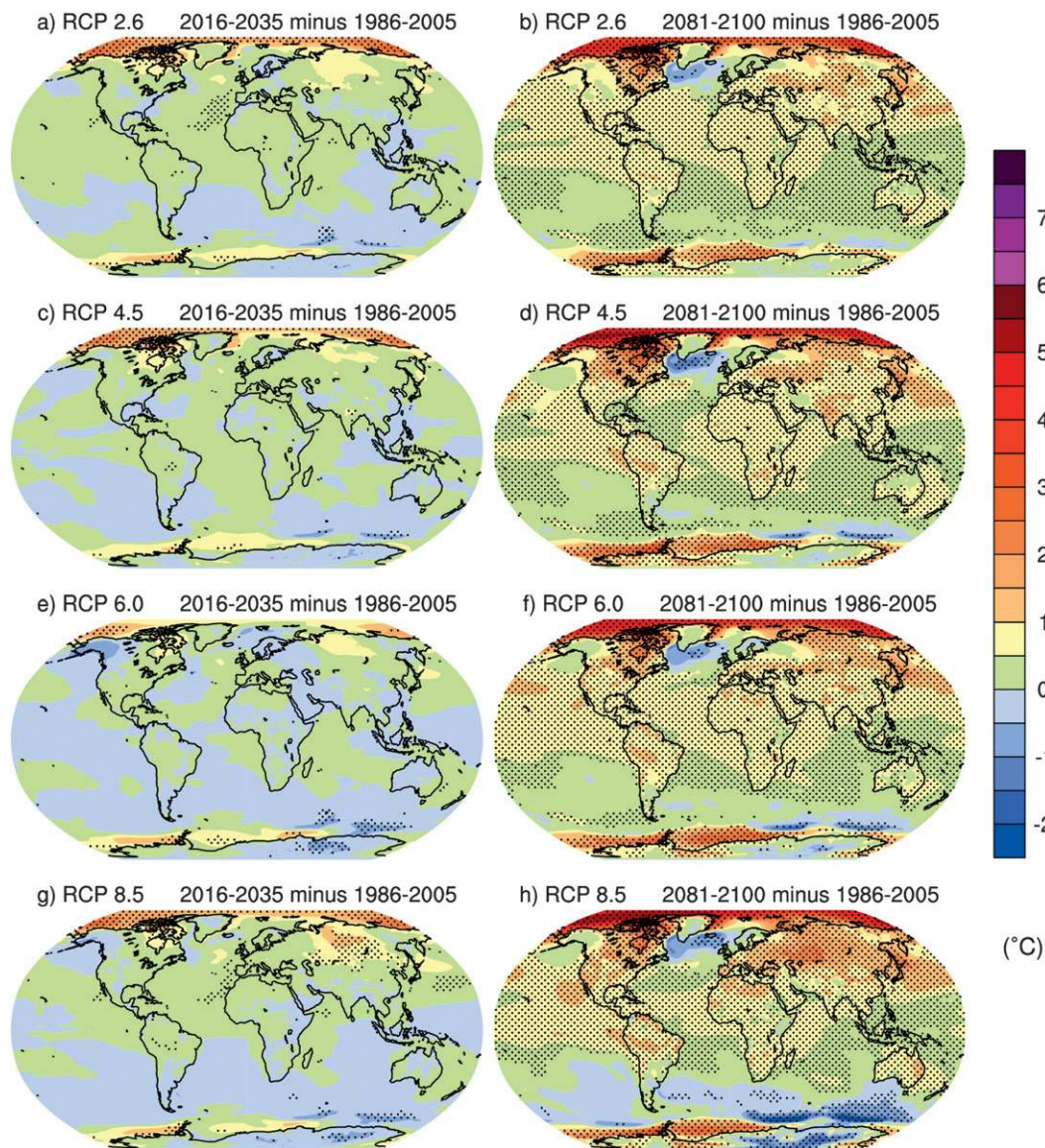
FIG. 4. CESM1(CAM5) − CCSM4 surface air temperature differences (°C) calculated in relation to a 1986–2005 base period, for (a),(b) RCP2.6, (c),(d) RCP4.5, (e),(f) RCP6.0, and (g),(h) RCP8.5 for two time periods: (left) near term (2016–35) and (right) longer term for the end of the twenty-first century (2081–2100). Ensemble mean changes from three [CESM1(CAM5)] and five (CCSM4) member ensembles are formed for each model prior to differencing. Stippling indicates statistical significance from a *t* test at the 5% level.

means (not shown) indicate a general response of wetter in the tropics and drier in the subtropics in CESM1(CAM5) compared to CCSM4, consistent with the response that could be expected with larger warming (Held and Soden 2006).

With regards to the monsoon simulations in the two models, the general seasonal mean patterns of precipitation for the monsoon regimes are similar in the two models [as shown for CCSM4 by Meehl et al. (2012c) and Cook et al. (2012)]. For future changes, both models show

slight enhancements of monsoon precipitation in JJA in the South Asian monsoon region, no significant changes in West African monsoon precipitation, and some indication of enhanced precipitation in the western region of the North American monsoon (Figs. 5b,d). For DJF, both models again show some increased precipitation in the Australian monsoon and parts of the South American monsoon regions (Figs. 5a,c). With regard to the differences between the models in future monsoon response, the enhancement of South Asian monsoon
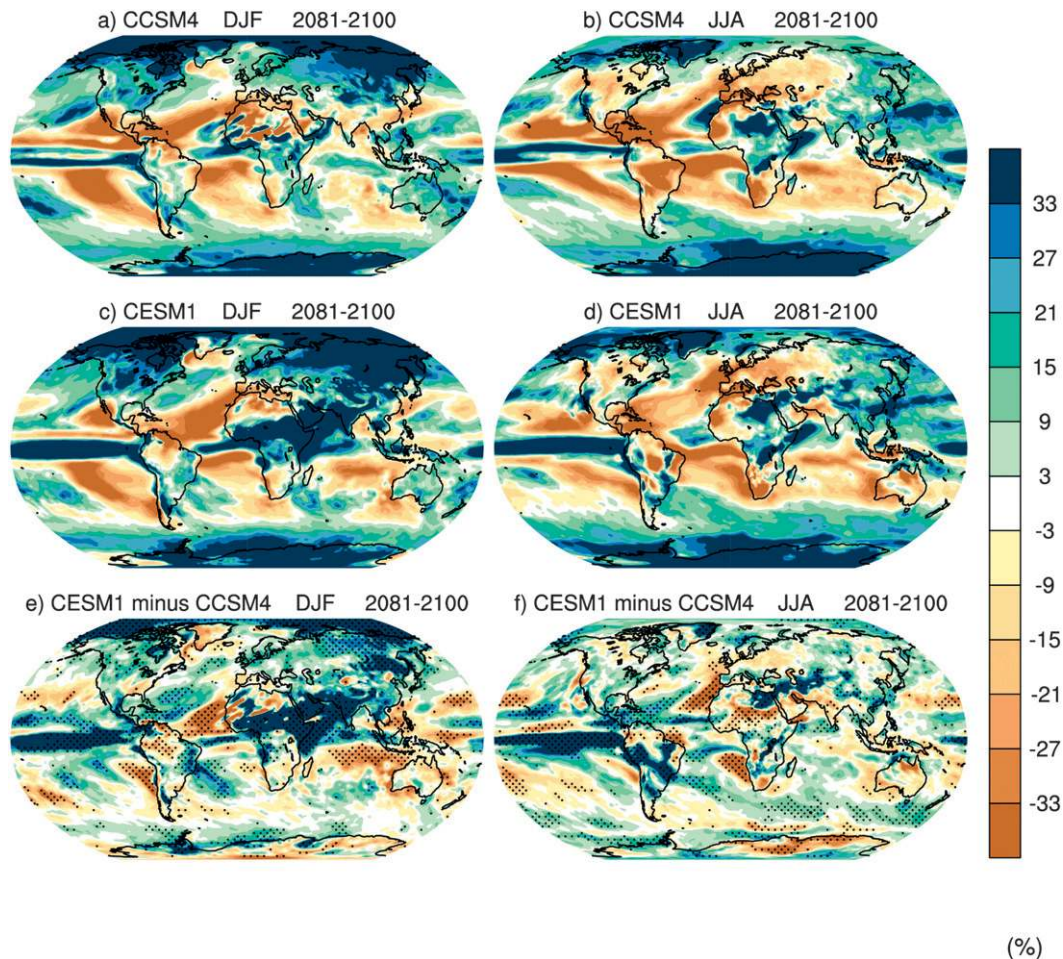
FIG. 5. Precipitation anomalies (%) for RCP8.5 (other scenarios have similar patterns with amplitude roughly scaled to temperature differences in the scenarios). (a) CCSM4, DJF, (2081–2100) − (1986–2005). (b) As in (a), but for JJA. (c) As in (a), but for CESM1(CAM5). (d) As in (b), but for CESM1(CAM5). (e) DJF, CESM1(CAM5) − CCSM4 [i.e., (c) − (a)]. (f) As in (e), but for JJA.

precipitation in CCSM4 is not as strong as in CESM1 (CAM5) (negative differences), with some relative decreases of West African monsoon precipitation and no significant changes of North American monsoon precipitation between the two models (Fig. 5f). For DJF in Fig. 5e, there is also relatively less Australian monsoon precipitation and South American monsoon precipitation over the Amazon region. Most notable are the wintertime relative increases in precipitation over West Africa and India in CESM1(CAM5) compared to CCSM4 (Fig. 5e).

With regards to sea level pressure (SLP) changes in Fig. 6 in CESM1(CAM5) compared to CCSM4, there is, in general, relatively lower pressure at high latitudes in each hemisphere even in the early period, indicating a shift to more positive phases of the northern annular mode (NAM) and southern annular mode (SAM) with greater increases of GHGs in CESM1(CAM5) (Arblaster

and Meehl 2006; Arblaster et al. 2011). Although this is not a strong signal in the geographical plots in Fig. 6, this is more evident in zonal mean changes of temperature and winds discussed below with regards to Fig. 7. With the greater tropical precipitation response in CESM1 (CAM5), relatively higher pressure dominates in most subtropical regions corresponding to a greater expansion of the Hadley cell in CESM1(CAM5) (e.g., Meehl et al. 2007). This is seen in Figs. 7c and d as a poleward shift of the subtropical jets particularly in the Northern Hemisphere signified by negative zonal wind differences near 30°N and positive zonal wind differences near 40°N. The large relative warming in the stratosphere could also have dynamical impacts on the circulation, as shown by Maycock et al. (2012) for the opposite case. There is higher SLP in the Asian–Australian region that is significant in the later period, indicative of a weakening of
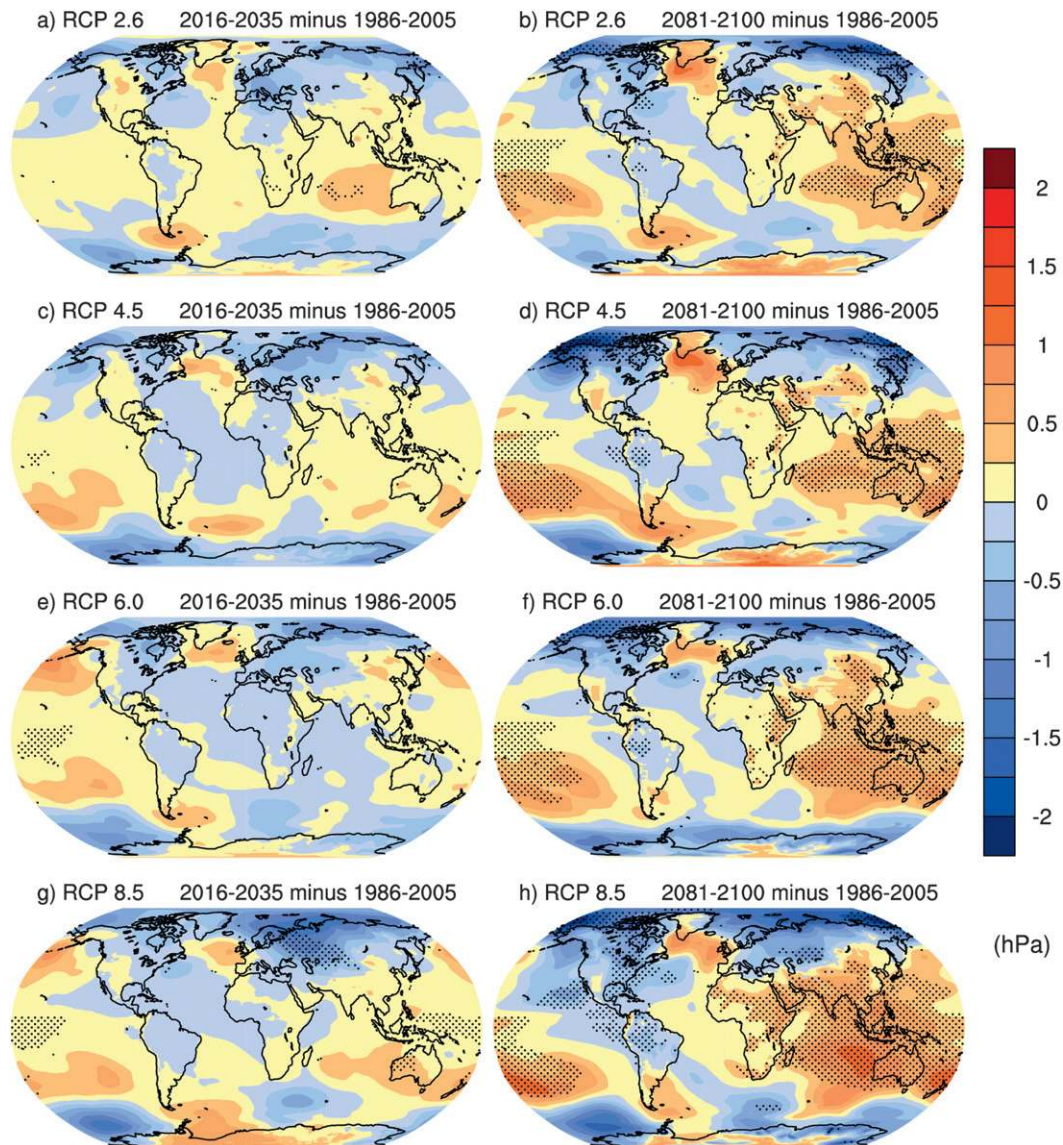
FIG. 6. As in Fig. 3, but for sea level pressure (hPa).

the Walker circulation that is also consistent with en-
hanced equatorial Pacific rainfall.

These changes in temperature and sea level pressure
are further illustrated by zonal mean cross sections of
temperature and wind differences (Fig. 7) to contrast the
RCP2.6 and RCP8.5 mitigation scenarios. Differences
for the DJF season are shown because in this season
stratospheric ozone recovery in the SH has its largest
impact on tropospheric climate (Thompson et al. 2011;
Eyring et al. 2013) and stratosphere–troposphere cou-
pling is most active in the NH (Manzini et al. 2013,
manuscript submitted to *J. Geophys. Res.*). There is
significant warming throughout the troposphere in the
midlatitudes of the NH, which is likely related to the

different treatment of aerosols in the two models (see
section 5). Some relative cooling is found aloft at high
latitudes, especially over the Arctic, where the surface
warming is more confined to the lower troposphere in
CESM1(CAM5). There is a relative increase in the me-
ridional temperature gradient in the CESM1(CAM5)
near 50°–60°N/S, and a greater poleward shift of the
midlatitude westerlies under both RCP2.6 and RCP8.5
at those latitudes. This is symptomatic of the tendency
toward a more positive phase of the NAM and SAM
noted in Fig. 6. In the Southern Hemisphere, apart from
an equatorward shift in the subtropical jet, differences
between the CESM1(CAM5) and CCSM4 projected
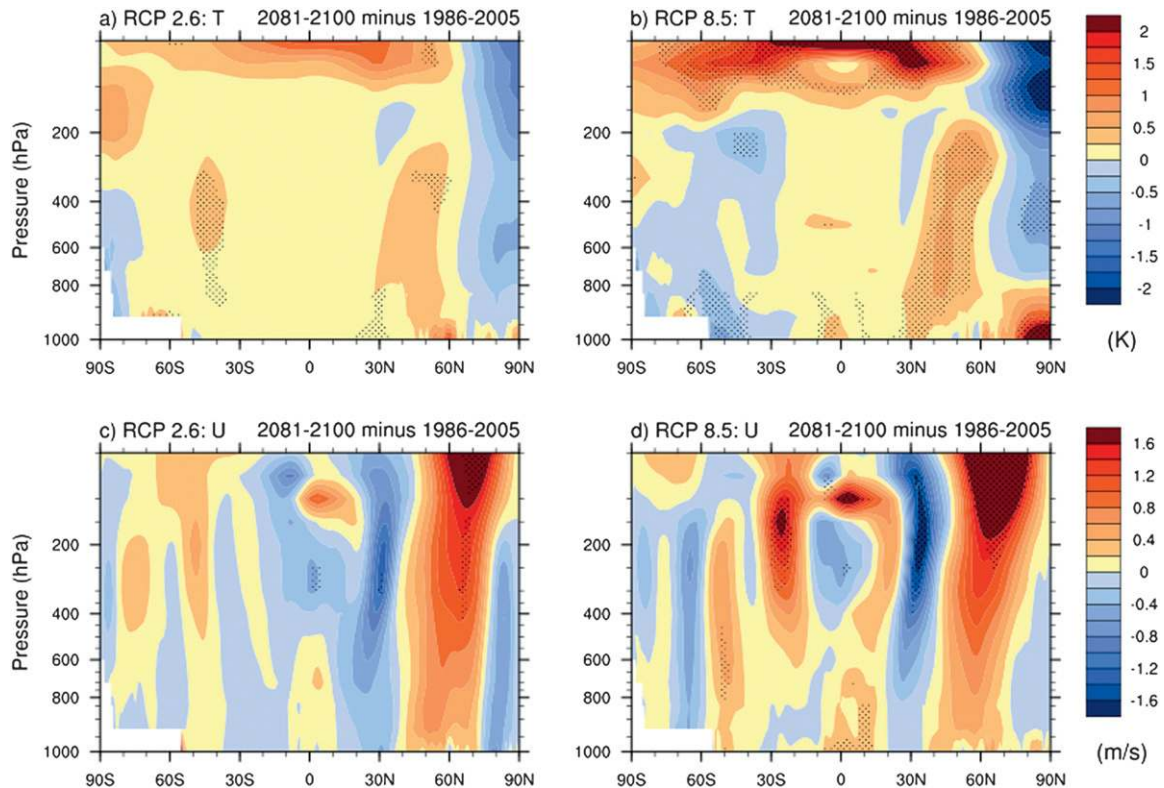changes in temperature are somewhat cooler in the

FIG. 7. CESM1(CAM5) − CCSM4 zonal mean DJF (top) temperature (°C) and (bottom) wind differences (m s^{-1}) for (left) RCP2.6 and (right) RCP8.5 for (2081–2100) − (1986–2005). Ensemble mean changes from three [CESM1(CAM5)] and six (CCSM4) member ensembles are formed for each model prior to differencing. Stippling indicates statistical significance from a *t* test at the 5% level.

SH (Fig. 4, left panels) but are mostly insignificant. This is possibly due to a larger response to ozone recovery (more stratospheric warming over Antarctica in Fig. 7b) offsetting the impacts of the greater climate sensitivity in CESM1(CAM5).

4. Response of the AMOC

The Atlantic meridional overturning circulation (AMOC) is defined here as the maximum of the zonal mean overturning streamfunction below 500 m in the Atlantic. In the preindustrial control run, the average value of this AMOC index is similar in CESM1(CAM5) and CCSM4, with a value of 24.1 Sv (1 Sv = 10^6 m^3 s^{-1}) in the CESM1(CAM5), compared to 25.0 Sv in the CCSM4. AMOC values at 25°N (near a number of observed estimates) are shown in Table 2 for the two models and some observational estimates near that latitude, and show reasonable correspondence between the computed and observed values. For reference to those values at 25°N, during the twentieth century for CESM1(CAM5), the mean overall maximum AMOC

(usually near 35° to 40°N) is 24.4 Sv (Fig. 8), and it is 24.3 Sv for CCSM4.

Jahn and Holland (2013) show that the strength of the AMOC decreases proportionally with the warming of the planet. Thus, as earth warms during the twentieth century, the AMOC magnitude decreases more in CCSM4 compared to CESM1(CAM5) in Fig. 8 because CCSM4 warms more during the twentieth century (R. B. Neale

TABLE 2. Values for AMOC in Sv at or near 25°N for (left) models and (right) observations.

|	
20.3 (CCSM4 control)	18.7 ±5.6 (at 26.5°N; Cunningham et al. 2007)
19.7 (CCSM4 twentieth century)	22.9, 18.7, 19.4, 16.1, 14.8 (at 25°N; Bryden et al. 2005)
	18 ±2.5 (at 24°N, inverse model; Lumpkin and Speer, 2007)
18.5 [CESM1(CAM5) control]	15 ±2 (North Atlantic, inverse model, North Atlantic Deep Water; Ganachaud and Wunsch 2000)
18.8 [CESM1(CAM5) twentieth century]	23 ±3 (at 30°S, inverse model, North Atlantic Deep Water; Ganachaud and Wunsch 2000)
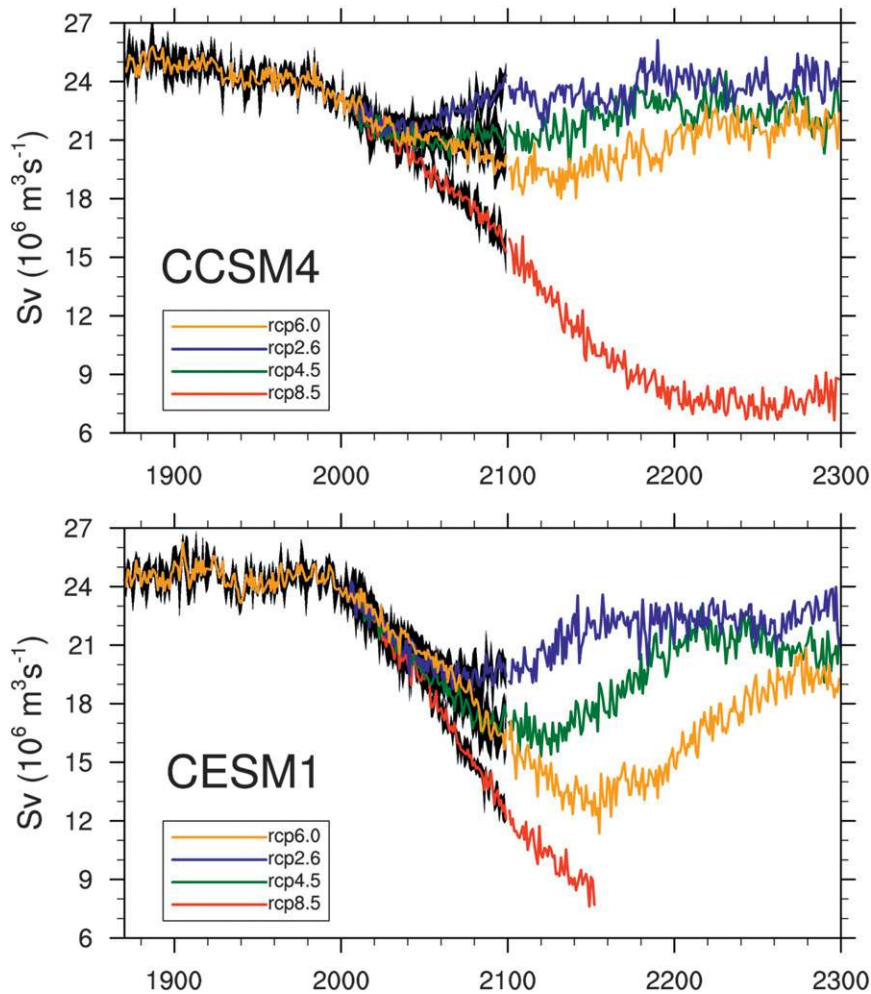
FIG. 8. Index of AMOC taken as the largest value of annual mean meridional overturning streamfunction below 500 m depth in Sv. Solid lines are ensemble averages for the twentieth and twenty-first centuries with shading indicating the range of the ensemble. After 2100, solid lines indicate single members: (a) CCSM4, five ensemble members; (b) CESM1(CAM5), three ensemble members.

et al. 2013, personal communication). But in CCSM4 the AMOC mostly recovers to mid-twentieth-century values in the RCP2.6, 4.5, and 6.0 simulations at some point before the end of the twenty-third century (Fig. 8b). This is because CCSM4 warms less than the corresponding CESM1(CAM5) simulations (Fig. 2). For example, in RCP2.6, in CCSM4 the AMOC only weakens to about 22 Sv in the early twenty-first century and has mostly recovered by 2100. However, in CESM1(CAM5) in RCP2.6, the AMOC reduces to about 19.5 Sv by around 2090 before starting to recover, and only returns to relatively stable values of around 22.5 Sv by 2200, below the twentieth-century average of about 24.4 Sv. Similarly for RCP4.5 and RCP6.0 in CESM1(CAM5), the AMOC weakens to values of about 16.5 and 13.0 Sv

near 2120 and 2140, respectively, only recovering to levels of about 21 and 19.5 Sv by 2220 and 2280, respectively. Jahn and Holland (2013) trace these differences to processes associated with a reduction of North Atlantic deep convection due to surface freshening. For example, deep ocean convection in the Labrador Sea is affected by decreases in Arctic sea ice cover that are associated with increased liquid freshwater exports into that region from the Arctic. Thus the greater Arctic warming in CESM1(CAM5) is associated with more sea ice melt (Fig. 11) and a larger amplitude weakening of the AMOC (Fig. 8). As noted by Jahn and Holland (2013), the biggest changes in Arctic sea ice occur in the summer season, and this is also seen in CCSM4 and CESM1(CAM5) (see Fig. 12). Thus, following Jahn
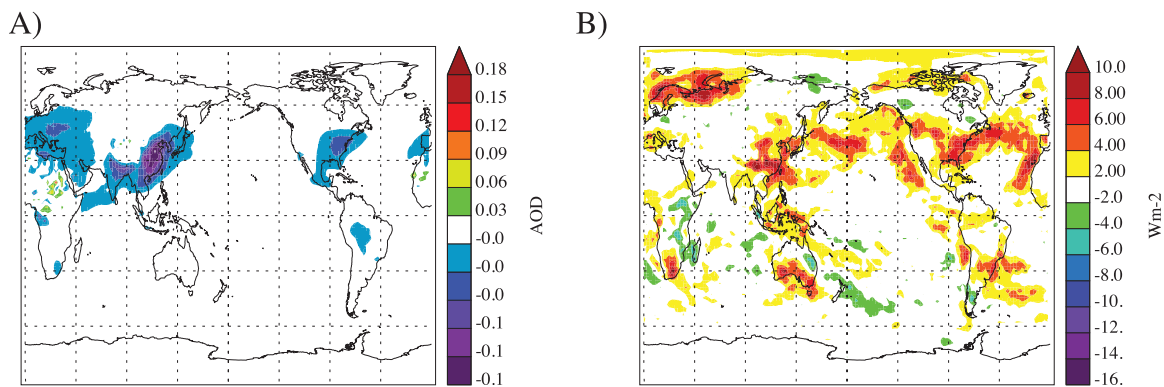
FIG. 9. Difference 2100 − 2005 emissions in CESM1(CAM5) fixed SST experiments for (a) aerosol optical depth (AOD) and (b) aerosol indirect effect as the change in cloud radiative effect (CRE).

and Holland (2013), the CESM1(CAM5) with greater warming and more melting of summer Arctic sea ice contributes to increased freshening in the North Atlantic, and a greater weakening and slower recovery of the AMOC (Fig. 8).

For the high forcing mitigation scenario RCP8.5, both CESM1(CAM5) and CCSM4 show a near shutdown of the AMOC by about 2200, with the shutdown occurring somewhat earlier in CESM1(CAM5), as could be expected from its larger warming response. As described by Jahn and Holland (2013) and Gent (2013), in the RCP8.5 simulations there is a complete shutdown of deep water formation in the Labrador Sea, Greenland–Iceland–Norwegian Seas, and Arctic Ocean due to the large increase in SSTs and freshening of the surface layer associated with the extensive sea ice melt. The CCSM4 RCP8.5 run has been continued out to 2500 with constant CO_2 forcing at year 2300 values to investigate whether the AMOC starts to recover. It does not, with AMOC index values north of 40°N hovering near 3 Sv out to 2500. Gent (2013) suggests that a further continuation of this run would produce comparably small AMOC values for several hundred years, with a recovery probably occurring only on the long diffusive time scales required for heat to reach the ocean mid-depths. This was also seen in the 5000-yr run of Stouffer and Manabe (2003).

5. Aerosol effects in CESM1(CAM5)

As has been noted above, a new feature in CESM1 (CAM5) compared to CCSM4 is that in the former there are prognostic aerosols that include both direct and indirect effects of aerosols, while in the latter aerosol concentrations were prescribed and included only the direct effect. The resulting difference in forcing in the simulations in the twenty-first century was noted above

to be ∼ +1 W m^{-2} Thus, effectively, the CESM1(CAM5) is experiencing a larger forcing (change in radiative flux) in the twenty-first century than CCSM4 due to the inclusion of the indirect effect in CAM5 as seen in Fig. 2. This can be partly explained by the larger forcing in CESM1(CAM5) due to reduction in indirect aerosol cooling, which is illustrated for the RCP8.5 case in Fig. 9b. The aerosol effects may also complicate or interact with cloud feedbacks, particularly in the Northern Hemisphere storm-track regions. As noted in Fig. 3, the slower rate of ocean heat uptake in CESM1(CAM5) also contributes to greater surface air temperature increase compared to CCSM4, but this likely has nothing to do with the different aerosol forcings since this characteristic of slower ocean heat uptake is seen in the 1% CO_2 increase experiment as well.

Some of the differences in the geographic patterns of warming in Fig. 4 have contributions from the changes in aerosol forcing. Figure 9 illustrates the change in aerosol optical depth (Fig. 9a) and the cloud radiative effect (CRE) associated with the direct and indirect forcing of aerosols. Here the indirect effect in CESM1 (CAM5) is mapped as the change in CRE (longwave and shortwave) in Fig. 9b. Maps of the effect as the residual of the total flux perturbation and the clear sky effect (TOA − FSC in Table 1) are similar. Differences in CRE are concentrated in the NH in and adjacent to source regions of aerosols over continents (chiefly North America, Europe, and East Asia) where the influence on temperature should be greatest. Indeed, the consequences of these changes in CRE are shown by surface air temperature differences over the oceans in the two hemispheres (Table 3). CESM1(CAM5) shows more warming over the NH oceans than the SH oceans for end of century, while CCSM4 is mostly the opposite (Table 3). With the reduction of the indirect and direct effect, the NH in CESM1(CAM5) experiences additional positive

TABLE 3. Surface air temperature differences (°C), (2081–2100) − (1986–2005) for CESM1(CAM5) and CCSM4 and the difference CESM1(CAM5) − CCSM4 for the SH and NH oceans and their difference for each scenario.

CESM1(CAM5)	RCP2.6	RCP4.5	RCP6.0	RCP8.5
NH Oceans	1.30	1.87	2.28	3.35
SH Oceans	1.11	1.77	2.10	3.11
Diff (NH − SH)	0.19	0.10	0.18	0.24
CCSM4	RCP2.6	RCP4.5	RCP6.0	RCP8.5
NH Oceans	0.73	1.32	1.64	2.73
SH Oceans	0.69	1.34	1.71	2.87
Diff (NH − SH)	0.03	−0.02	−0.07	−0.14
CESM1(CAM5) − CCSM4	RCP2.6	RCP4.5	RCP6.0	RCP8.5
NH Oceans	0.58	0.56	0.64	0.62
SH Oceans	0.42	0.44	0.39	0.24
Diff (NH − SH)	0.16	0.12	0.25	0.39

indirect forcing (e.g., Fig. 9b) and so the NH in CESM1(CAM5) responds by warming more over the oceans than in CCSM4 by the end of the twenty-first century.

The reasons for the geographic distribution of the AOD contrast between models in Fig. 9 are related to different estimates of emissions, mainly in regions of industrial pollution, but also in regions of biomass burning like the Amazon. Additionally, the indirect effect is largest in regions of high AOD as could be expected, but there are also some effects in remote regions in the SH where the air is relatively pristine. This is likely the result of teleconnections as well as interannual variations in cloud forcing.

Aerosol forcing may also influence the vertical structure of temperature changes by affecting the cloud forcing. In Fig. 7 there are significantly larger mid-tropospheric temperature changes in CESM1(CAM5) in the Northern Hemisphere that are particularly notable in late century. These changes likely have a contribution from the reductions in direct and indirect effects of aerosols, since more solar radiation penetrates the atmosphere in 2100 than in 2006.

6. Projected changes in Arctic and Antarctic regions

To evaluate projected transient changes in Arctic surface temperatures and sea ice extent in CESM1(CAM5) and CCSM4, Fig. 10 shows that annual mean twenty-first-century Arctic (70°–90°N) warming (2081–99 minus 2006–25) is greater in CESM1(CAM5) (9°C) than in CCSM4 (7°C) in RCP8.5. Figure 10 also shows that annual mean and September Arctic sea ice loss occurs more rapidly in CESM1(CAM5) than in CCSM4.
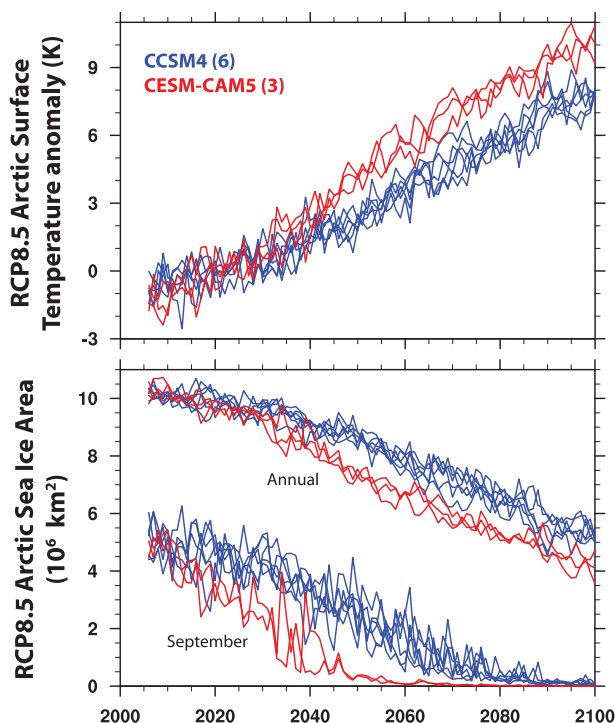

FIG. 10. Arctic time series for the RCP8.5 forcing scenario: (a) Surface air temperature anomaly relative to 2006–2035 base period (°C). (b) Annual mean and September Arctic sea-ice area (10^6 km²).

Indeed, the Arctic becomes ice-free during September in RCP8.5 in the 2040s in CESM1(CAM5) as compared to the 2060s in CCSM4. The larger projected changes in Arctic climate in CESM1(CAM5) as compared to CCSM4 are in contrast to their similarly reasonable twentieth-century simulations of seasonal variations of sea ice extent and sea ice thickness distributions as evaluated against available observations (R. B. Neale et al. 2013, personal communication). Consistent with analysis of slab ocean carbon dioxide doubling experiments in Kay et al. (2012), larger radiative forcing from increased greenhouse gases and stronger positive shortwave feedbacks resulting from less negative short-wave cloud feedbacks and more positive shortwave surface albedo feedbacks both help explain the greater Arctic change in CESM1(CAM5) than in CCSM4 (not shown).

To provide a more comprehensive comparison of Arctic sea ice changes over the historical period and under different forcing scenarios, Fig. 11 shows time series of average ice extent for the Arctic for the seasons February–April (FMA) and August–October (ASO). These times of year are selected because they are when the sea ice is at its seasonal maximum and minimum extent. Over the late twentieth century, both observations
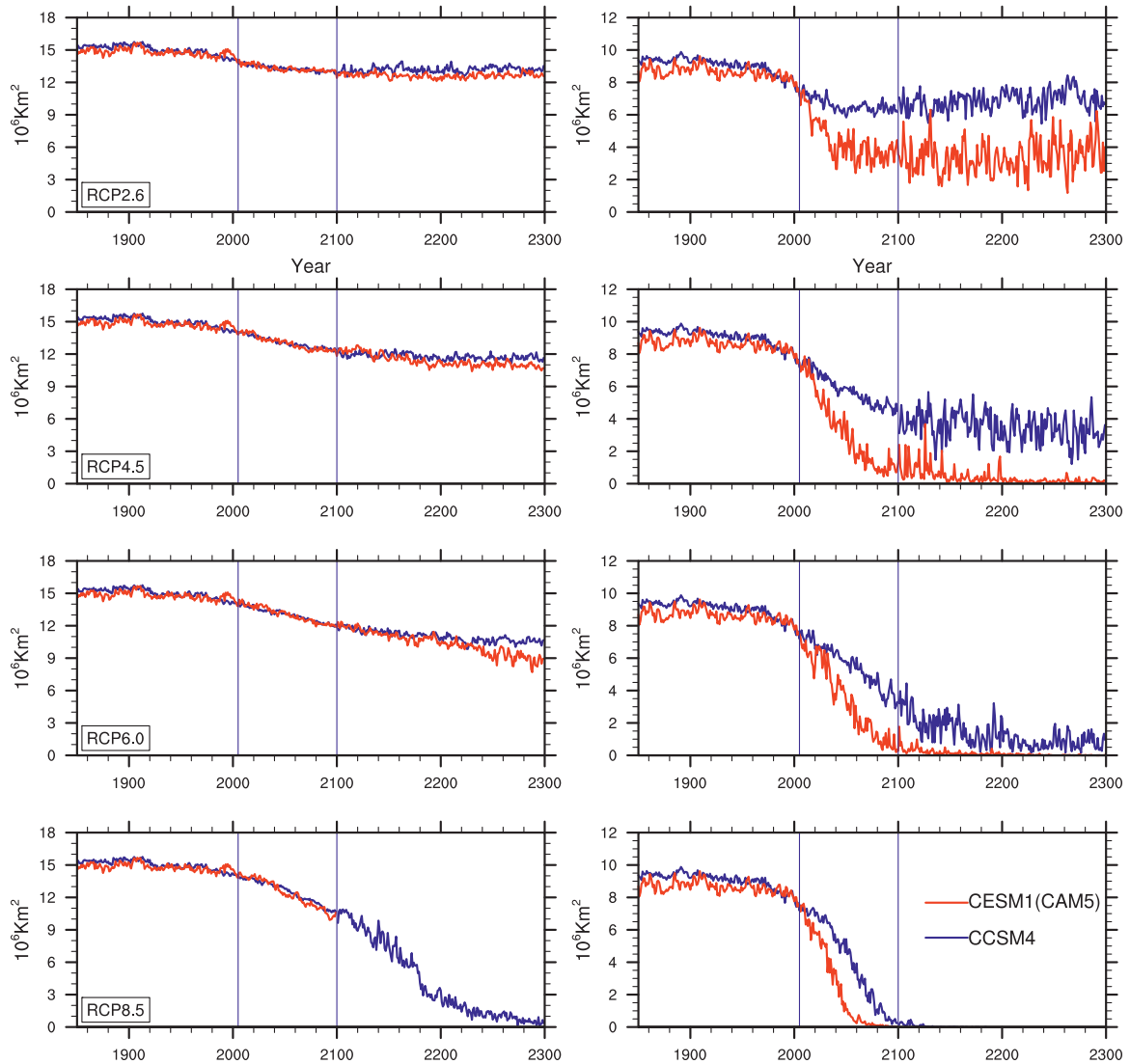
FIG. 11. Ensemble average Arctic sea ice extent (10^6 km^2) for CCSM4 (blue line) and CESM1(CAM5) (red line) for (left) the February–April (FMA) season and (right) the August–October (ASO): season (top to bottom) RCP2.6, RCP4.5, RCP6.0, and RCP8.5. For CESM1(CAM5) these are averages of three ensemble members from 1850–2100, and one each for the extensions beyond 2100, and an ensemble average of five members for CCSM4.

and the models show declines in Arctic sea ice extent, with the Arctic sea ice extent in ASO decreasing at about the same rate as observations. There are hints of improvement in CESM1(CAM5) over CCSM4 where the ASO Arctic sea ice was decreasing faster than the observations (Meehl et al. 2012a, their Fig. 19), although the substantial influence of internal variability on Arctic sea ice trends (e.g., Kay et al. 2011) has not yet been investigated.

For the sea ice trends in future climate projections, RCP8.5 shows a near vanishing of ASO season-average Arctic sea ice by about 2080, with a nearly ice-free Arctic in ASO in the two intermediate scenarios, RCP4.5

and RCP6.0, by the end of the century. Only in the low scenario, RCP2.6, does ASO Arctic sea ice extent stabilize by midcentury with about half the present-day extent in CESM1(CAM5). Beyond 2100 in CESM1(CAM5), there is a nearly ice-free summer Arctic after 2100 in RCP6.0 and after 2120 in RCP4.5, but ice extent stabilizes and even increases slightly by 2300 to values near 4×10^6 km^2 in RCP2.6 (Fig. 10). For RCP2.6 in Fig. 11, and similar to the AMOC in Fig. 8, there is a larger rate of decrease of summer sea ice area in CESM1(CAM5) in the Arctic with a slower recovery in CESM1(CAM5). The more rapid approach to an ice-free summer Arctic by 2100 in the two intermediate scenarios RCP4.5 and
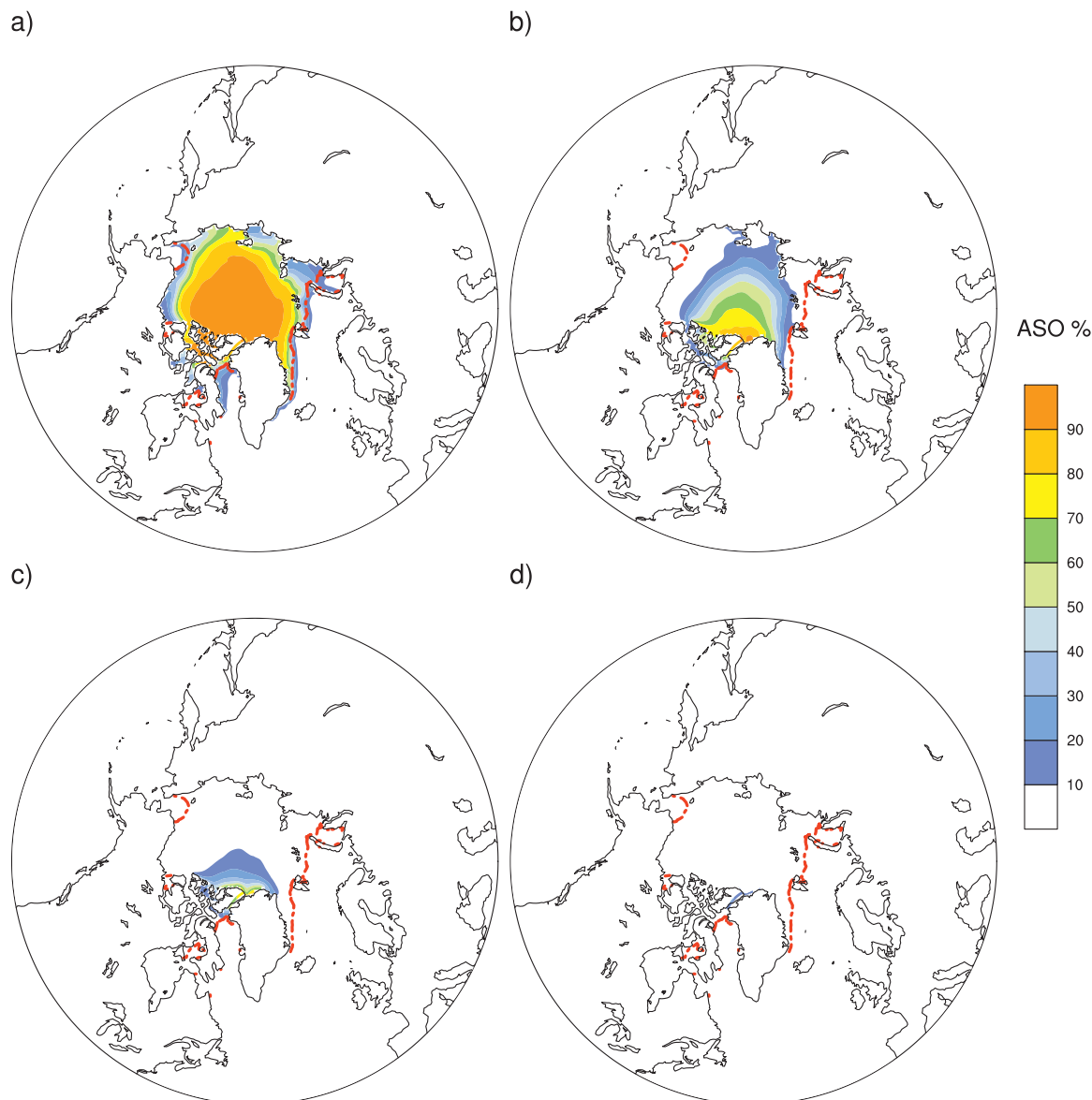
a)

b)

ASO %

c)

d)

FIG. 12. For CESM1(CAM5), ASO Arctic (a) late-twentieth-century (1986–2005 average) sea ice concentration (%), (b) late-twenty-first-century (2081–2100 average) sea ice concentration for RCP2.6, (c) late-twenty-first-century (2081–2100 average) sea ice concentration for RCP4.5, and (d) late-twenty-first-century (2081–2100 average) sea ice concentration for RCP8.5. Dash-dotted red line is observed sea ice extent for end of twentieth century.

RCP6.0 is evident, compared to the much less rapid loss of summer sea ice in CCSM4. Similar to Fig. 10, an earlier ice-free Arctic summer season during ASO occurs much earlier in CESM1(CAM5) than in CCSM4 (40 yr). For the FMA season, both models respond similarly with relatively small decreases of ice extent of around 10% by 2100, and only a further loss of sea ice of another 15% or less by 2300 depending on the scenario. There is substantial sea ice remaining during winter by 2300 in both models.

To give a geographic perspective on Arctic sea ice transient changes, Figs. 12 and 13 show polar projection plots of ASO Arctic sea ice extent for a recent period (1986–2005) along with ice extent for three of the RCP scenarios (RCP2.6, RCP4.5, and RCP8.5). The dash-dotted red line shows the observed present-day extent of sea ice in the Arctic. For the 2081–2100 average, RCP8.5 in CESM1(CAM5) shows no ASO sea ice remaining (Fig. 12d) while in CCSM4 there is still a small amount left (Fig. 13d). Meanwhile in the intermediate RCP4.5
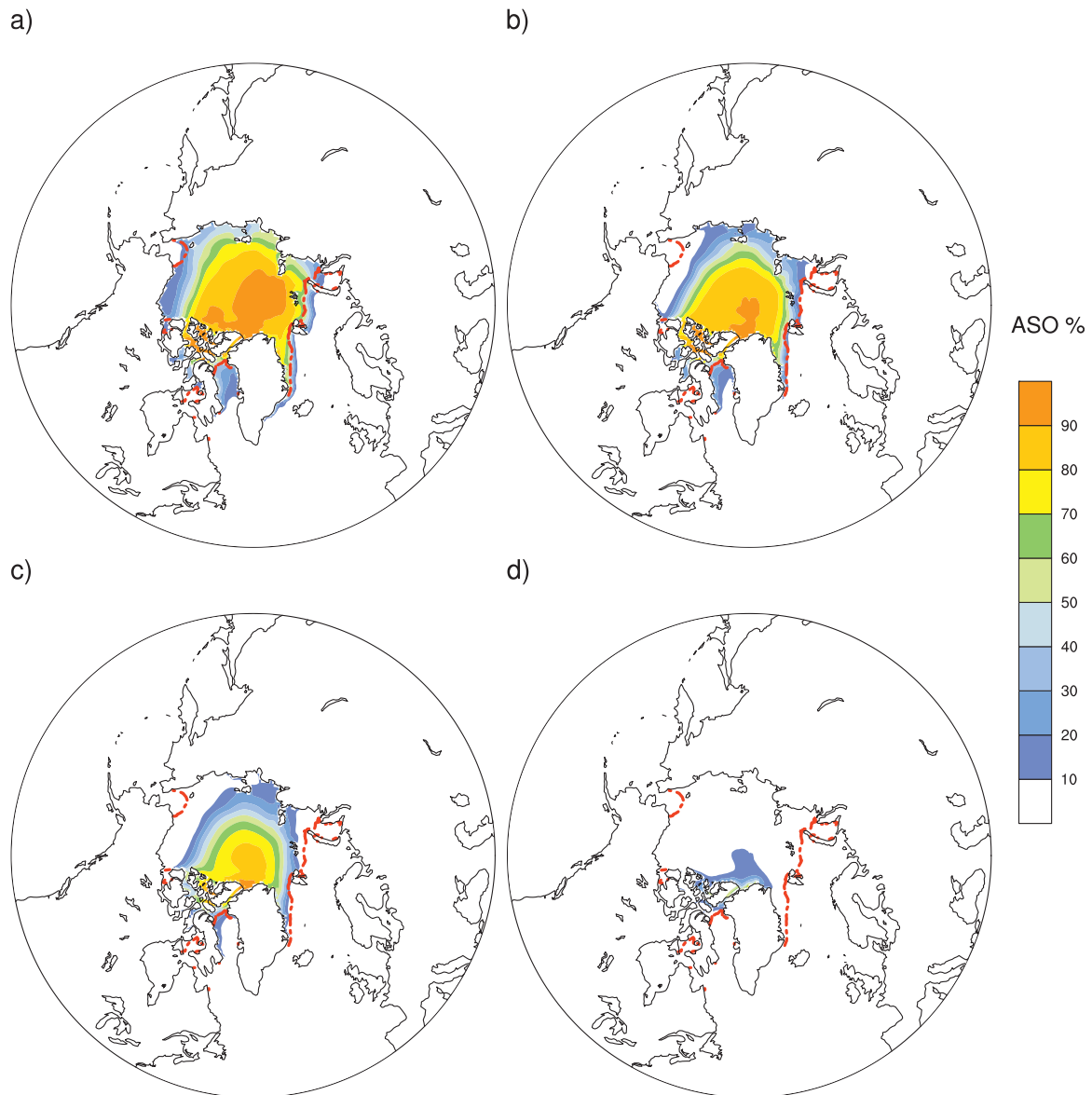
a)

b)

c)

d)

ASO %

FIG. 13. As in Fig. 12, but for CCSM4.

scenario for CESM1(CAM5), there is almost as little sea ice left in ASO (Fig. 12c) as in the high scenario for RCP8.5 in CCSM4 (Fig. 13d). In CCSM4 with the aggressive mitigation scenario in RCP2.6 where CO_2 concentrations are decreasing by the end of the century, much more sea ice remains in ASO (Fig. 13b) than in the CESM1(CAM5) (Fig. 12b). Therefore, with regard to summer Arctic sea ice in the twenty-first century, it makes a difference not only which future climate change scenario is followed, but also the climate sensitivity of the model being considered. CESM1(CAM5) with higher climate sensitivity shows larger future climate changes occurring sooner than in CCSM4 (Kay et al. 2012).

Transient changes in Arctic permafrost conditions are shown in Fig. 14 as trends in the integrated area in which permafrost is found in CCSM4 and CESM1(CAM5) within the top 3.8 m of soil. The observed estimate for late twentieth-century total permafrost extent (continuous and discontinuous permafrost) is $16.2 \times 10^6 \, \text{km}^2$. This value is derived from the gridded International Permafrost Association permafrost map and represents the area where 50% or more of the ground is underlain by permafrost, which is the relevant statistic against which large-scale models should be compared. The late-twentieth-century (1970–90) total permafrost extent is improved in CESM1(CAM5) (14.0 million km^2)
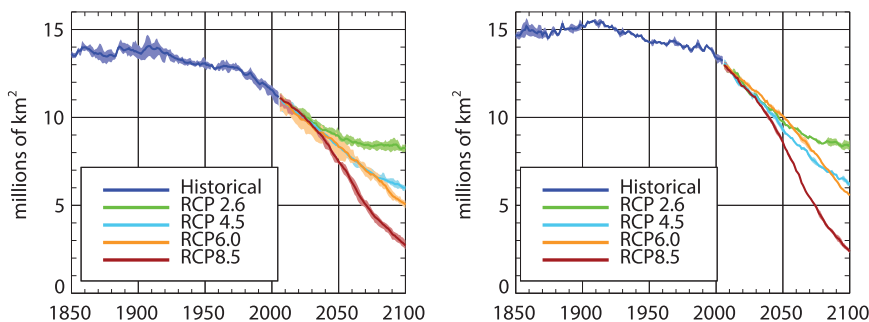
FIG. 14. Time series of NH near-surface permafrost extent for (left) CCSM4 and (right) CESM1(CAM5) for historical and projection periods. Near-surface permafrost extent is the integrated area of grid cells with at least one soil layer within the top 10 soil layers (3.8 m) that remains frozen throughout the year. Frozen ground underneath glaciers is not included in the near-surface permafrost extent. Shading indicates the ensemble spread [five members for CCSM4, two members for CESM1(CAM5)].

compared to CCSM4 (12.5 million km^2). The low bias in permafrost extent in CCSM4 is attributed at least partly to biases in the simulated Arctic climate over the permafrost domain, particularly excessive snowfall (D. M. Lawrence et al. 2012). The snowfall and snow depth biases are reduced in CESM1(CAM5), which leads to weaker winter and spring snow insulation of the soil, cooler soil temperatures, and more extensive permafrost.

The amount of projected near-surface permafrost loss as diagnosed both directly and indirectly in the CMIP5 models varies widely (Slater and Lawrence 2013; Koven et al. 2013) due to differences in the quality of the land models and differences in the basic state and trends in Arctic climate simulated by the GCMs. CCSM4, which appears to be among the better models when it comes to representing permafrost in a global coupled climate model, exhibits trends in twenty-first-century near-surface permafrost extent that are roughly in the middle of the range of projected trends across all the models. The projected twenty-first-century permafrost losses in CESM1(CAM5), however, are considerably stronger than in CCSM4, reflecting the greater Arctic warming in CESM1(CAM5). The total near-surface permafrost area loss for 2005 to 2100 for RCP8.5 is 27% greater in CESM1(CAM5) than in CCSM4 (10.8 vs 8.5 × 10^6 km^2). In both CESM1(CAM5) and CCSM4, near-surface permafrost extent stabilizes by 2100 in RCP2.6 at just over 8 × 10^6 km^2, though the areal loss from 2005 to 2100 is greater by about 1.8 × 10^6 km^2 in CESM1(CAM5).

For the Antarctic, Fig. 15 shows Antarctic sea ice projections in CESM1(CAM5) and CCSM4 for the twentieth century and the four RCP scenarios. In the Antarctic region, CESM1(CAM5) sea ice extent is a much closer match to the observations than the overextensive

Antarctic CCSM4 sea ice simulations (see R. B. Neale et al. 2013, personal communication, and Meehl et al. 2012a, Fig. 19). The reduced and therefore improved Antarctic sea ice mean extent in CESM1(CAM5) as compared to CCSM4 is partly a result of a reduction in mean wind stress in the Southern Ocean (R. B. Neale et al. 2013, personal communication). Despite the improved mean state in CESM1(CAM5), both CCSM4 and CESM1(CAM5) simulate decreasing Antarctic sea ice area at the end of the twentieth century in contrast to observations that show slight statistically insignificant increases of Antarctic sea ice area. The reasons for this are under investigation. Into the mid and late twenty-first century, CESM1(CAM5) and CCSM4 show ongoing decreases in Antarctic sea ice, with the greatest losses in RCP8.5 during FMA. This is occurring even as surface westerlies are increasing somewhat (Fig. 7), which should contribute to increasing sea ice extent. At the same time surface temperatures are however increasing, so it appears that the warming ocean in the model is contributing to a future melt-back of Antarctic sea ice; this is enough to offset the effect of increasing surface winds that would act to increase sea ice extent. Antarctic sea ice extent is stabilized in RCP2.6 in both seasons and both models after 2100, but continues to slowly decline in RCP4.5 and RCP6.0 in winter and summer. Antarctic summer (FMA) sea ice in CESM1(CAM5) is totally gone in RCP8.5 by about 2200, and stabilizes in winter at a low value by about 2250.

For RCP2.6 in Fig. 15, and similar to the AMOC in Fig. 8 and for Arctic sea ice in Fig. 11, there is a larger rate of decrease of summer sea ice area in CESM1(CAM5) in the Antarctic (Fig. 15c) with a slower recovery in CESM1(CAM5). For RCP8.5 in Fig. 15, there is an ice-free Antarctic summer season about 50 years earlier in CESM1(CAM5).
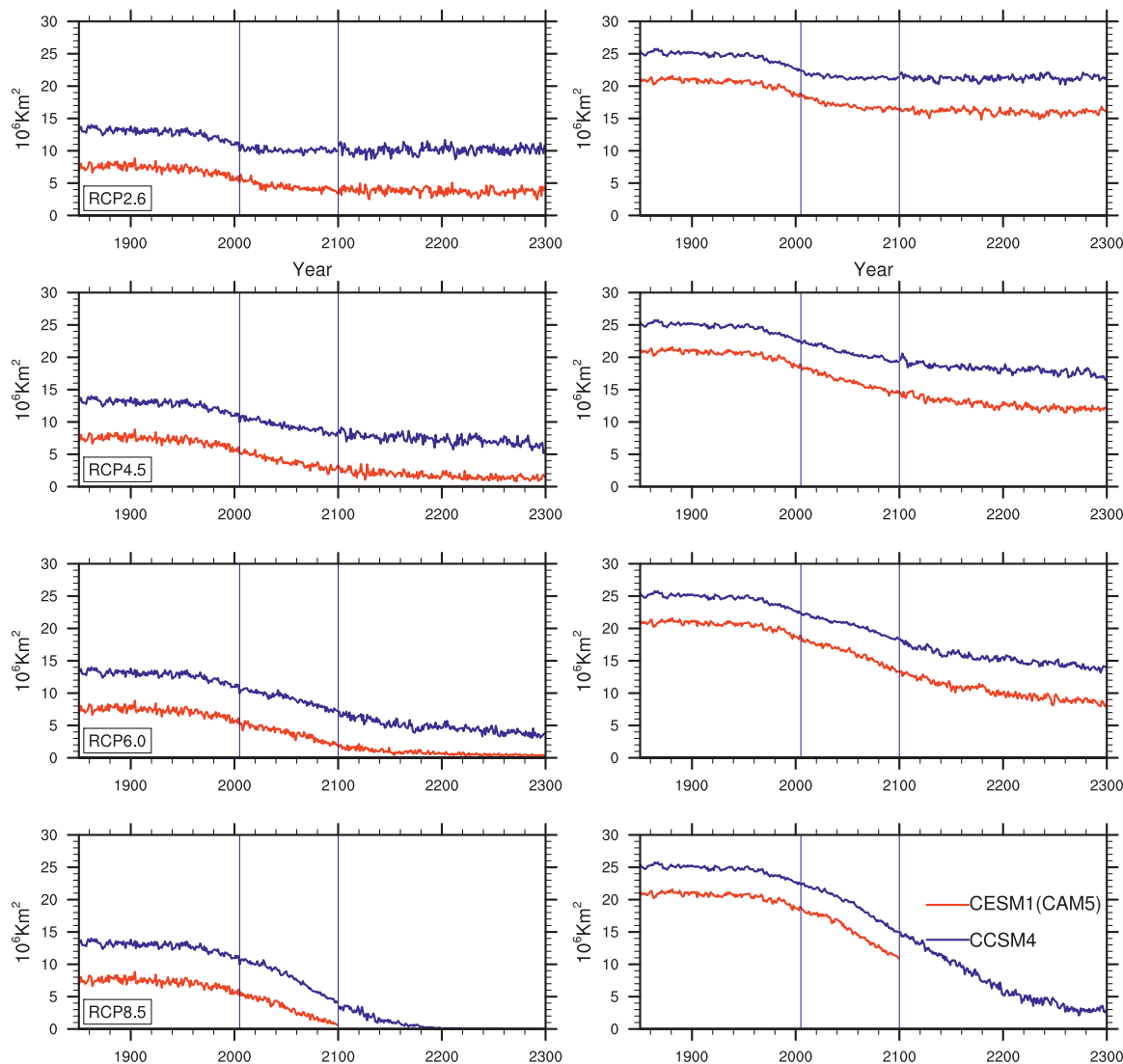
FIG. 15. As in Fig. 11, but for Antarctic sea ice extent.

7. Discussion

Although the land, ocean, and sea ice components are the same in CCSM4 and CESM1(CAM5), the improvements in a number of parameterizations in CAM5 provide a more realistic model and an improved simulation of twentieth-century climate in CESM1(CAM5). Because of stronger feedbacks, CESM1(CAM5) has higher ECS and TCR, with the latter increasing more in proportion to equilibrium climate sensitivity in CESM1(CAM5) due to a slower rate of ocean heat uptake. This factor, with contributions from weaker winds and AMOC in CESM1(CAM5), combined with the inclusion of the aerosol indirect effect in that model, produces larger-amplitude climate changes in

the twenty-first century and beyond in CESM1(CAM5) compared to CCSM4. In particular, a curious consequence of including the indirect effect is that the twentieth-century climate is cooler in CESM1(CAM5) and closer to observations than in CCSM4, but as the aerosol burden decreases in the twenty-first century, there is greater warming in CESM1(CAM5) due to its higher climate sensitivity.

In almost all respects, therefore, there are larger responses in all parameters in the future climate in that model compared to CCSM4, with greater warming, larger precipitation and sea level pressure changes, an earlier ice-free summer Arctic, and more rapid loss of permafrost. With the greater realism of the CESM1(CAM5), these changes could be viewed as more credible than in

CCSM4, although both models, in terms of ECS and TCR, are in the range of what is estimated to be the actual values of those metrics. Thus, both models contribute to the range of responses in the parameter space populated by the larger multimodel ensemble of CMIP5.

Finally, both models show that the climate system is committed, right now, to further ongoing climate change in the future even if concentrations can be stabilized in the RCP scenarios. This emphasizes once again that the longer we wait to act to mitigate emissions of GHGs, the more difficult it will be to eventually stabilize climate change.

8. Conclusions

The Community Earth System Model version 1 (CESM1) that includes the Community Atmospheric Model version 5 (CAM5), referred to herein as CESM1 (CAM5), has been run for future climate change projections following the experiment design of phase 5 of the Coupled Model Intercomparison Project (CMIP5). These results are compared to the previous model version, the Community Climate System Model version 4 (CCSM4). Results are shown for the four Representative Concentration Pathway (RCP) mitigation scenarios, and extensions of those scenarios beyond 2100 to 2300. The ECS of CESM1(CAM5) is 4.10°C, which is higher than the CCSM4 value of 3.20°C. The TCR in CESM1(CAM5) is also higher than in CCSM4, with a value for the former of 2.33°C, compared to the latter with a value of 1.73°C. The TCR in CESM1(CAM5) is also proportionately greater than ECS compared to CCSM4, and this is traced to slower heat uptake in the former model that contributes to greater warming of surface air temperature. An additional factor that makes CESM1(CAM5) more responsive to changes in external forcings is that it includes both the direct and indirect effects of aerosols (CCSM4 had only the direct effect). This contributes to an additional transient indirect forcing in the RCP scenarios of up to $1.2\,\mathrm{W\,m^{-2}}$ as anthropogenic aerosols are projected to decline by 2100 to 20% of current levels (80% reduction). Thus, the response of the climate system in CESM1(CAM5) is affected by slower ocean heat uptake, higher climate sensitivity, and increased forcing, resulting in an overall future climate system response to increasing greenhouse gases that is greater compared to CCSM4. Global surface temperatures averaged for the last 20 years of the twenty-first century compared to the 1986–2005 reference period for three member ensembles from CESM1(CAM5) are +1.49°, +2.31°, +2.75°, and +4.13°C for RCP2.6, RCP4.5, RCP6.0, and RCP8.5, respectively,

while comparable values for CCSM4 are +0.85°, +1.64°, +2.09°, and +3.53°C. Although the Atlantic Ocean meridional overturning circulation (AMOC) weakens during the twentieth century in CCSM4, there is little trend in CESM1(CAM5). The future AMOC behavior is also quite different in CESM1(CAM5), with the AMOC weakening considerably in the twenty-first century in all the RCP scenarios, and recovering more slowly in the lower forcing scenarios compared to CCSM4. The reduction in aerosol indirect forcing contributes to additional warming, especially over the Northern Hemisphere oceans in CESM1(CAM5). The magnitude is consistent with expectations from decreases in aerosol indirect forcing and the different climate sensitivity. This warming that is concentrated in the NH impacts Arctic temperatures, and likely affects sea ice extent as well. Sea ice extent in the twentieth-century simulations of CESM1(CAM5) is close to observed, as in CCSM4, but is significantly improved compared to CCSM4 around Antarctica with a reduced sea ice extent in CESM1(CAM5) in closer agreement to observations. However, as in CCSM4, the recent trend of decreasing Antarctic sea ice extent in CESM1(CAM5) is not reflected in observations. CESM1(CAM5) shows a greater sea ice loss in the Arctic in the summer season compared to CCSM4, with an ice-free summer Arctic occurring by about 2060 in RCP8.5 in CESM1(CAM5) as opposed to about 2100 in CCSM4. There are also nearly ice-free summer conditions in the lower forcing scenarios of RCP4.5 and RCP6.0 by about 2100 compared to much more sea ice being retained in those scenarios in CCSM4. When compared to CCSM4, there is more Arctic warming and sea ice loss in CESM1(CAM5). This greater Arctic response results from larger CO_2 radiative forcing and stronger shortwave feedbacks in CESM1(CAM5) as compared to CCSM4.

REFERENCES

Andrews, T., J. M. Gregory, M. J. Webb, and K. E. Taylor, 2012: Forcing, feedbacks and climate sensitivity in CMIP5 coupled atmosphere–ocean climate models. *Geophys. Res. Lett.,* **39,** L09712, doi:10.1029/2012GL051607.

Arblaster, J. M., and G. A. Meehl, 2006: Contribution of various external forcings to trends in the southern annular mode. *J. Climate,* **19,** 2896–2905.

——, ——, and D. Karoly, 2011: Future climate change in the Southern Hemisphere: Competing effects of ozone and greenhouse gases. *Geophys. Res. Lett.,* **38,** L02701, doi:10.1029/ 2010GL045384.

Bitz, C. M., K. M. Shell, P. R. Gent, D. Bailey, G. Danabasoglu, K. C. Armour, M. M. Holland, and J. T. Kiehl, 2012: Climate sensitivity of the Community Climate System Model version 4. *J. Climate,* **25,** 3053–3070.

Brohan, P., J. J. Kennedy, I. Harris, S. F. B. Tett, and P. D. Jones, 2006: Uncertainty estimates in regional and global observed temperature changes: A new dataset from 1850. *J. Geophys. Res.,* **111,** D12106, doi:10.1029/2005JD006548.

Bryden, L. H., H. R. Longworth, and S. A. Cunningham, 2005: Slowing of the Atlantic meridional overturning circulation at 25°N. *Nature,* **438,** 655–657, doi:10.1038/nature04385.

Cavalieri, D. J., C. L. Parkinson, P. Gloersen, J. C. Comiso, and H. J. Zwally, 1999: Deriving long-term time series of sea ice cover from satellite passive-microwave multisensor data sets. *J. Geophys. Res.,* **104,** 15 803–15 814.

Cook, K. H., G. A. Meehl, and J. M. Arblaster, 2012: Monsoon regimes and processes in CCSM4. Part II: The African and American monsoons. *J. Climate,* **25,** 2609–2621.

Cunningham, S. A., and Coauthors, 2007: Temporal variability of the Atlantic meridional overturning circulation at 26.5°N. *Science,* **317,** 935–938.

Eyring, V., and Coauthors, 2010: Sensitivity of 21st century stratospheric ozone to greenhouse gas scenarios. *Geophys. Res. Lett.,* **37,** L16807, doi:10.1029/2010GL044443.

——, and Coauthors, 2013: Long-term ozone changes and associated climate impacts in CMIP5 simulations. *J. Geophys. Res. Atmos.,* **118,** 5029–5060, doi:10.1002/jgrd.50316.

Ganachaud, A., and C. Wunsch, 2000: Improved estimates of global ocean circulation, heat transport and mixing from hydrographic data. *Nature,* **408,** 453–457.

Gent, P. R., 2013: Coupled models and climate projections. *Ocean Circulation and Climate,* 2nd ed., Academic Press, in press.

——, and Coauthors, 2011: The Community Climate System Model version 4. *J. Climate,* **24,** 4973–4991.

Gettelman, A., H. Morrison, and S. J. Ghan, 2008: A new two-moment bulk stratiform cloud microphysics scheme in the NCAR Community Atmosphere Model (CAM3). Part II: Single-column and global results. *J. Climate,* **21,** 3660–3679.

——, and Coauthors, 2010: Global simulations of ice nucleation and ice supersaturation with an improved cloud scheme in the community atmosphere model. *J. Geophys. Res.,* **115,** D18216, doi:10.1029/2009JD013797.

——, J. E. Kay, and K. M. Shell, 2012a: The evolution of climate sensitivity and climate feedbacks in the Community Atmosphere Model. *J. Climate,* **25,** 1453–1469.

——, X. Liu, D. Barahona, U. Lohmann, and C. Chen, 2012b: Climate impacts of ice nucleation. *J. Geophys. Res.,* **117,** D20201, doi:10.1029/2012JD017950.

——, J. E. Kay, and J. T. Fasullo, 2013: Spatial decomposition of climate feedbacks in the Community Earth System Model. *J. Climate,* **26,** 3544–3561.

Held, I. M., and B. J. Soden, 2006: Robust responses of the hydrological cycle to global warming. *J. Climate,* **19,** 5686–5699.

Jahn, A., and M. M. Holland, 2013: Implications of Arctic sea ice changes for North Atlantic deep convection in CCSM4-CMIP5 simulations. *Geophys. Res. Lett.,* **40,** 1206–1211, doi:10.1002/grl.50183.

Kay, J. E., M. M. Holland, and A. Jahn, 2011: Inter-annual to multi-decadal Arctic sea ice extent trends in a warming world. *Geophys. Res. Lett.,* **38,** L15708, doi:10.1029/2011GL048008.

——, ——, C. Bitz, E. Blanchard-Wrigglesworth, A. Gettelman, A. Conley, and D. Bailey, 2012: The influence of local feedbacks and northward heat transport on the equilibrium Arctic climate response to increased greenhouse gas forcing in coupled climate models. *J. Climate,* **25,** 5433–5450.

Koven, C. D., W. J. Riley, and A. Stern, 2013: Analysis of permafrost thermal dynamics and response to climate change in the CMIP5 Earth system models. *J. Climate,* **26,** 1877–1900.

Lamarque, J.-F., and Coauthors, 2010: Historical (1850–2000) gridded anthropogenic and biomass burning emissions of reactive gases and aerosols: Methodology and application. *Atmos. Chem. Phys.,* **10,** 7017–7039, doi:10.5194/ acp-10-7017-2010.

——, G. P. Kyle, M. Meinshausen, K. Riahi, S. J. Smith, D. P. van Vuuren, A. Conley, and F. Vitt, 2011: Global and regional evolution of short-lived radiatively-active gases and aerosols in the representative concentration pathways. *Climatic Change,* **109,** 191–212, doi:10.1007/s10584-011-0155-0.

Lawrence, D. M., and Coauthors, 2011: Parameterization improvements and functional and structural advances in version 4 of the Community Land Model. *J. Adv. Model. Earth Syst.,* **3,** M03001, doi:10.1029/2011MS000045.

——, A. G. Slater, and S. C. Swenson, 2012: Simulation of present-day and future permafrost and seasonally frozen ground conditions in CCSM4. *J. Climate,* **25,** 2207–2225.

Lawrence, P. J., and Coauthors, 2012: Simulating the biogeochemical and biogeophysical impacts of transient land cover change and wood harvest in the Community Climate System Model (CCSM4) from 1850 to 2100. *J. Climate,* **25,** 3071–3095.

Liu, X., and Coauthors, 2012: Toward a minimal representation of aerosols in climate models: Description and evaluation in the Community Atmosphere Model CAM5. *Geosci. Model Dev.,* **5,** 709–735, doi:10.5194/gmd-5-709-2012.

Lumpkin, R., and K. Speer, 2007: Global ocean meridional overturning. *J. Phys. Oceanogr.,* **37,** 2550–2562.

Maycock, A. C., M. M. Joshi, K. P. Shine, and A. A. Scaife, 2012: The circulation response to idealized changes in stratospheric water vapor. *J. Climate,* **26,** 545–561.

Meehl, G. A., W. M. Washington, W. D. Collins, J. M. Arblaster, A. Hu, L. E. Buja, W. G. Strand, and H. Teng, 2005: How much more global warming and sea level rise? *Science,* **307,** 1769–1772.

——, and Coauthors, 2007: Global climate projections. *Climate Change 2007: The Physical Science Basis.* S. Solomon et al., Eds., Cambridge University Press, 747–845.

——, and Coauthors, 2012a: Climate system response to external forcings and climate change projections in CCSM4. *J. Climate,* **25,** 3661–3683.

——, and Coauthors, 2012b: Relative outcomes of climate change mitigation related to temperature versus sea level rise. *Nat. Climate Change,* **2,** 576–580, 10.1038/nclimate1529.

——, J. M. Arblaster, J. Caron, H. Annamalai, M. Jochum, A. Chakraborty, and R. Murtugudde, 2012c: Monsoon regimes and processes in CCSM4. Part I: The Asian–Australian monsoon. *J. Climate,* **25,** 2583–2608.

Morrison, H., and A. Gettelman, 2008: A new two-moment bulk stratiform cloud microphysics scheme in the NCAR Community Atmosphere Model (CAM3). Part I: Description and numerical tests. *J. Climate,* **21,** 3642–3659.

Moss, R., and Coauthors, 2010: The next generation of scenarios for climate change research and assessment. *Nature,* **463,** 747–756, doi:10.1038/nature08823.

Neale, R. B., and Coauthors, 2010: Description of the NCAR Community Atmosphere Model (CAM5.0). NCAR Tech. Rep. NCAR/TN-486+STR, 268 pp.

Sanderson, B. M., and K. M. Shell, 2013: Model specific radiative kernels for calculating cloud and noncloud feedbacks. *J. Climate,* **25,** 7607–7624.

Slater, A. G., and D. M. Lawrence, 2013: Diagnosing present and future permafrost from climate models. *J. Climate,* **26,** 5608–5623.

Stouffer, R. J., and S. Manabe, 2003: Equilibrium response of thermohaline circulation to large changes in atmospheric CO_2 concentration. *Climate Dyn.,* **20,** 759–773.

Taylor, K. E., R. J. Stouffer, and G. A. Meehl, 2012: The CMIP5 experiment design. *Bull. Amer. Meteor. Soc.,* **93,** 485–498.

Thompson, D. W. J., S. Solomon, P. J. Kushner, M. H. England, K. M. Grise, and D. J. Karoly, 2011: Signatures of the Antarctic ozone hole in Southern Hemisphere surface climate change. *Nat. Geosci.,* **4,** 741–749.

van Vuuren, D. P., and Coauthors, 2011: The representative concentration pathways: An overview. *Climatic Change,* **109,** 5–31, doi:10.1007/s10584-011-0148-z.